ASTROPARTICLE PHYSICS

I. Tkachev
Theory Division, CERN, CH-1211 Geneva 23, Switzerland
and
Institute for Nuclear Research of the Russian Academy of Sciences, 117312, Moscow, Russia

Abstract
In this astro-particle lecture course I shall try to emphasize evidence of the new physics which we have in cosmological and astrophysical data. This includes support of the inflationary model, necessity of dark energy and of non-baryonic dark matter, the Grizen-Zatsepin-Kuzmin puzzle of the ultra-high energy cosmic rays.

1. INTRODUCTION

The purpose of these CERN school lectures is to review the evidence for the new physics in cosmological and astrophysical data, and to give the minimal theoretical frameworks needed to understand and appreciate the evidence. Beyond any reasonable doubt, we have solid evidence for the new physics in these data. The strongest is the case for non-baryonic dark matter, followed by the case for dark energy. The possibility (though very speculative, since a consistent and working model has not been constructed yet) that the law of gravity should be changed instead is not excluded, but that would mean a new physics anyway. I will not engage in discussion of relevant particle physics model building, instead the reader is refereed to lectures by G. Gabadadze at this school [1]. Another solid evidence for the new physics beyond the standard model is given by neutrino oscillations. I will not discuss this topic, it is covered in lectures by S. Petcov at this school [2]. The physics of cosmic rays is partially covered in lectures by A. Chilingaryan [3], therefore, I restrict myself to the highest-energy part of the spectrum, which is related to Grizen-Zatsepin-Kuzmin puzzle and, possibly, to a new physics.

There are many excellent reviews on the subject of Cosmology and Astroparticle physics, including lectures at previous CERN schools, for a recent one see [4, 5, 6]. I've tried to be complimentary to these lectures to the extent it is possible, so many additional details can be found there. Proceedings of these schools can be found at http://physicschool.web.cern.ch/PhysicSchool. Due to space and time limitations, I omit several very important traditional topics, most notably Big Bang Nucleosynthesis (see e.g. the review [7]) and Baryogenesis (see e.g. the review [8]). In the area covered, I've updated experimental results and resulting constraints, where applicable. The most important developments since the time of the previous school were: release of the first year observations of Cosmic Microwave Background Radiation (CMBR) by the Wilkinson Microwave Anisotropy Probe (WMAP) [9], first data release by the Sloan Digital Sky Survey (SDSS) of three-dimensional distribution of galaxies [10], and the release[11] of a statistically significant dataset of Supernovae Ia at large cosmological redshifts, $z > 1$, which provide the first conclusive evidence for cosmic deceleration that preceded the current epoch of cosmic acceleration. These are long awaited cosmological data of unprecedented quality, and with their appearance cosmology has truly entered the golden era and became a precision science.

The plan of the lectures is as follows. In Section 2., I review the basics of cosmology: Friedman equations, Hubble expansion, cosmography. In Section 3., the Cosmic Microwave Background Radiation (CMBR) is discussed. In Section 4., I briefly review resent results on another cosmological probe - the large-scale distribution of galaxies. In Section 5., the evidence for the existence of dark energy is presented. Sections 6. and 6.3 review the evidence for a dark matter, and particle physics models of non-baryonic matter are briefly considered. In Section 7., I review the basics of inflationary cosmology and discuss support of the inflationary model by the CMBR data. In Section 8., the physics of the Ultra-high energy cosmic rays is reviewed.

2. BASICS OF COSMOLOGY

2.1 Note on units and scales

Length. Astronomers are measuring distances in parsecs, which is about 3.1×10^{16} m or about 3.26 light years, and is comparable with the distance to the closest star. PARSEC is an abbreviation for the distance to a star with a semi-annual PARallax of 1 arc SECond. The distance from our Sun to the Galactic center is 8 kiloparsecs, so the kpc is an appropriate unit when discussing galactic structure. The appropriate unit of extragalactic distance, however, is the megaparsec, or Mpc. The nearest large cluster of galaxies, the Virgo cluster, is at a distance of 20 Mpc. The size of the visible Universe is 4200 Mpc or 13.7 billions of light years.

Energy. Usually astronomers are measuring energy in ergs. E.g. the luminosity of our Sun is $4 \times 10^{33}\ \mathrm{erg\ s^{-1}}$, while luminosity of bright quasars reaches $10^{46}\ \mathrm{erg\ s^{-1}}$. Galaxy like our Milky Way contains 10^{11} stars, and there are 10^{11} galaxies in the visible part of the Universe. Particle physicists are measuring energy in electron-volts, 1 erg $= 6.2 \times 10^{11}$ eV, and usually are choosing units where the velocity of light and the Plank constant are set to unity, $c = 1,\ \ \hbar = 1$, which I am using too, when convenient. In these units, for example, 1 Mpc $= 1.6 \times 10^{29}\ \mathrm{eV^{-1}}$.

2.2 Dynamical Frameworks

Dynamics is provided by General Relativity - the Einstein field equations

$$R_{\mu\nu} - \frac{1}{2} g_{\mu\nu} R = 8\pi G\, T_{\mu\nu}\ , \tag{1}$$

where $T_{\mu\nu}$ is a stress energy tensor describing the distribution of mass in space, G is Newton's gravitational constant, and the curvature $R_{\mu\nu}$ is a complicated function of the metric and its first and second derivatives. Clearly, finding a general solution to a set of equations as complex as the Einstein field equations is a hopeless task. The problem is simplified greatly considering mass distributions with special symmetries. The basic assumption underlying the construction of cosmological models is that of spatial homogeneity and isotropy. The most general space-time metric consistent with these symmetries is the Robertson-Walker metric:

$$ds^2 = dt^2 - a^2(t)\ \mathbf{dl}^2\ , \tag{2}$$

where $a(t)$ is the dimensionless scale factor by which all distances vary as a function of cosmic time t. The scale factor contains all the dynamics of the Universe, while the vector product $\mathbf{dl}^2$ describes the geometry of the space,

$$\mathbf{dl}^2 = \frac{dr^2}{1 - k\, r^2} + r^2\, (d\theta^2 + \sin^2\theta\, d\phi^2)\ ,$$

which can be either Euclidian, or positively or negatively curved. For the spatial 3-dimensional curvature we find, explicitly

$${}^{(3)}R = \frac{6k}{a^2(t)} \quad \begin{cases} k = -1 & \text{Open} \\ k = 0 & \text{Flat} \\ k = +1 & \text{Closed} \end{cases} \tag{3}$$

E.g., the space with $k = +1$ can be thought of as a 3-dimensional sphere with a curvature being inversely proportional to the square of its radius. In this Section we will model the matter content of the Universe as a perfect fluid with energy density ρ and pressure p, for which the stress-energy tensor in the rest frame of the fluid is

$$T_\mu^{\ \nu} = \begin{pmatrix} \rho & 0 & 0 & 0 \\ 0 & -p & 0 & 0 \\ 0 & 0 & -p & 0 \\ 0 & 0 & 0 & -p \end{pmatrix} \tag{4}$$

With these assumptions the Einstein equations simplify to the Friedmann equations, which form the dynamical basis of cosmology

$$\frac{\dot{a}^2}{a^2} = \frac{8\pi G}{3}\rho - \frac{k}{a^2}\,, \tag{5}$$

$$\frac{\ddot{a}}{a} = -\frac{4\pi G}{3}\left(\rho + 3\,p\right). \tag{6}$$

Let us have a look at the basic physics behind of these equations.

1. Differentiating Eq. (5) and subtracting Eq. (6) we obtain

$$\frac{d\rho}{dt} + 3\,\frac{\dot{a}}{a}\left(\rho + p\right) = 0\,, \tag{7}$$

which is nothing but energy-momentum conservation,

$$T_{\mu}^{\ \nu}{}_{;\nu} = 0\,. \tag{8}$$

On the other hand, the result is nothing but the First Law of thermodynamics

$$dE + p\,dV = T\,dS\,, \tag{9}$$

with $dS = 0$. Here $E = \rho V = \rho a^3 V_0$ is energy, T is temperature and S is entropy of some (fixed) comoving volume V_0. Therefore, Friedmann expansion driven by an ideal fluid is isentropic, $dS = 0$. This is not unexpected, and relaxing the assumption of a perfect fluid will lead to entropy production. However, the dissipation is negligible in cosmological frameworks (except of special moments, like the initial matter creation and possible phase transitions, which will be considered separately) and isentropic expansion is a very good approximation. This gives a useful integral of the motion, $S = \text{const}$. On dimensional grounds, $S \propto T^3 a^3 V_0$ and we obtain frequently used relation between the scale factor and temperature in an expanding Universe

$$a \propto \frac{1}{T}\,. \tag{10}$$

To be precise,

$$S = \frac{2\pi^2}{45}\,g_*\,T^3\,a^3 = \text{const}\,, \tag{11}$$

where the factor g_* counts the effective number of relativistic degrees of freedom

$$g_* = \sum_{i=\text{bosons}} g_i + \frac{7}{8}\sum_{j=\text{fermions}} g_j \equiv \left(g_B + \frac{7}{8}g_F\right). \tag{12}$$

At any given temperature, only particles with $m \ll T$ should be counted, i. e. g_* is a function of temperature, which is shown in Fig. 1. For a gas of photons, $g_* = 2$. Considering the current epoch of the Universe evolution, we have to add the neutrino contribution, which will be discussed later and leads to a different account of effective degrees of freedom at temperatures below e^+e^- annihilation in entropy, g_S, and in energy density, g_ρ. Namely, $g_S(T_0) = 3.909$ and $g_\rho(T_0) = 3.363$. At temperatures above the electroweak scale $g_* \sim 100$ in the Standard Model.

Let us give here also other thermodynamical relations, similar to Eq. (11), but for the energy density, ρ, and particle number density, n

$$\rho = \frac{\pi^2}{30}\,g_* T^4\,, \tag{13}$$

$$n = \frac{\zeta(3)}{\pi^2}\left(g_B + \frac{3}{4}g_F\right)T^3\,, \tag{14}$$

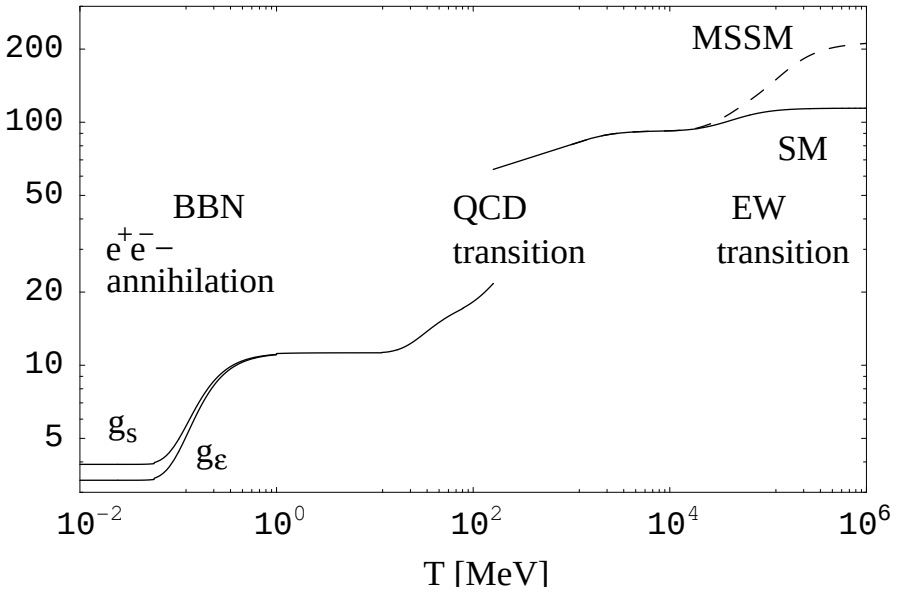

Fig. 1: Number of relativistic degrees of freedom as a function of temperature. From Ref. [12].

where $\zeta(3) = 1.202$. These relations are a simple consequence of the integration of Bose-Einstein or Fermi-Dirac distributions

$$\frac{g}{(2\pi)^3}\int \frac{d^3q}{\mathrm{e}^{q/T}\pm 1}\, q^a\,, \tag{15}$$

where q is particle momentum, the plus (minus) sign corresponds to fermions (bosons), and $a = 1$ in calculation of ρ, while $a = 0$ in calculation of n (in the latter case the integral cannot be evaluated in terms of elementary functions and the Riemann ζ-function appears). With the use of Eq. (9), the entropy density, Eq. (11), can be found as $s = 4\rho/3T$, since for the relativistic particles $p = \rho/3$ regardless of spin.

2. Friedmann equation, Eq. (5), can be interpreted within Newtonian mechanics. Indeed, let us first re-arrange it as

$$\frac{1}{2}\,\dot{a}^2 - \frac{4\pi G}{3}\,\rho\, a^2 = -\frac{k}{2}\,. \tag{16}$$

Now, it is easy to see that for $r = a\, r_0$, the Friedmann equation takes the form of energy conservation for test particles bounded in the gravitational potential created by mass $M = \frac{4\pi}{3}\,\rho\, r^3$,

$$\frac{1}{2}\,\dot{r}^2 - \frac{G\,M}{r} = -\frac{k\, r_0^2}{2}\,. \tag{17}$$

We see that the constant k, which determines the sign of spacial curvature in the language of General relativity, also determines the sign of the binding energy

$k = +1$	Binding energy is negative, the Universe will recollapse
$k = -1$	Binding energy is positive, the Universe will expand forever

Therefore, the case of zero spatial curvature, or zero binding energy, $k = 0$, is special and corresponds to fine tuning between initial kinetic and potential energies. Setting $k = 0$ in Eq. (5), this fine tuning can

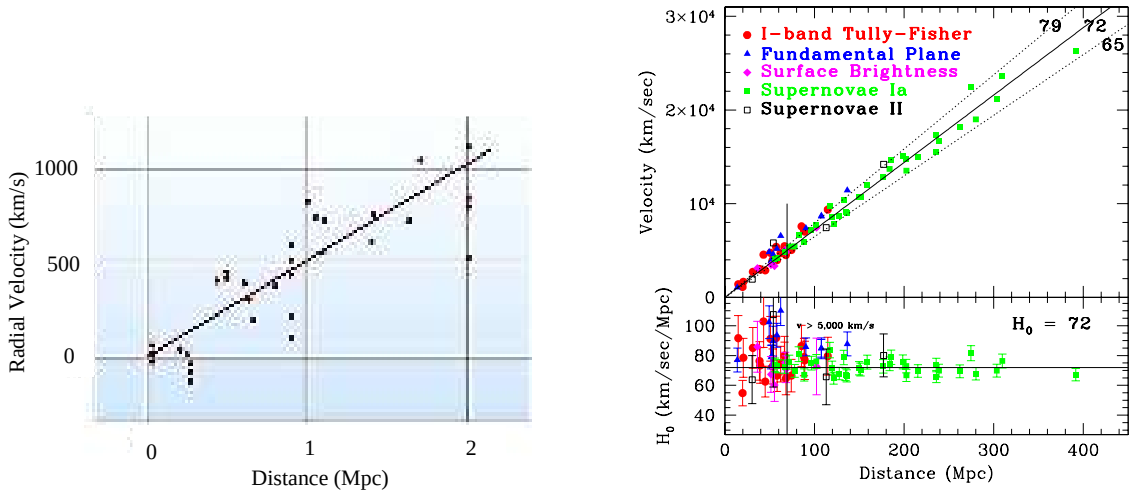

Fig. 2: Hubble Diagram. From Ref. [14].

be expressed as $\rho = \rho_c$, where the critical density is defined as

$$\rho_c \equiv \frac{3}{8\pi G} \left(\frac{\dot{a}}{a}\right)^2 . \tag{18}$$

The critical density is proportional to the square of another fundamental parameter,

$$H \equiv \frac{\dot{a}}{a} . \tag{19}$$

The present value of this parameter is called the Hubble constant. It describes the rate of the Universe expansion, and can be related to observations in the following way. Consider two points with a fixed comoving distance r_0 between them (this means that points do not feel any other forces and do not participate in any other motion beyond general expansion of the Universe). The physical distance between points increases as $r(t) = a(t)r_0$, and we can find the relative velocity as

$$v \equiv \dot{a}r_0 = \frac{\dot{a}}{a} ar_0 = Hr . \tag{20}$$

The relation $v = Hr$ is called the Hubble law. This is shown in Fig. 2. The left panel is original data used by E. Hubble, the right panel presents recent data from Ref. [13]. We will discuss it in more detail later on, especially in relation to observations. But the first thing we may notice is that according to Hubble law, $v \sim 1$ at $r \sim H^{-1}$. Separations (or wavelengths) of this order are therefore special in cosmology and mean *super-horizon* length scale. At smaller separations, Newtonian gravity should be valid. Einstein equations tell us that energy conservation in Newtonian mechanics, Eq. (5), and the first law of thermodynamics, Eq. (7), applied to the Universe as a whole, can be extended beyond horizons without any change. The second Friedmann equation, Eq. (6), can be derived as a consequence of these two equations. However, hardly would Newton do it, even if he had known the first law of thermodynamics. Indeed, in Eq. (6) we recognize the Newton's second law, $F = m\dot{v}$ with F being the gravity force, and energy conservation is derived from the equations of motion, not vice versa.

We see that, according to Einstein's theory, the force law is modified. Not only mass gravitates, but the pressure, too, gives its contribution into gravitational force. This is a very important modification, since pressure can be negative, leading to anti-gravity and to accelerated expansion. As we will see, this stage of expansion may have lead to creation of the Universe in our classical understanding. At present,

the Universe expansion seems to be dominated by anti-gravity as well. This has an interesting history. Newton did not know that one should worry about horizons, but he worried why the Universe does not collapse under the pull of gravity. Einstein was worried about this too. He added (1917) a cosmological constant to the equations of motion, thinking that it will make the Universe static. (As we will see, the cosmological constant corresponds to a vacuum with non-zero energy density and negative pressure, $p = -\rho$.) However, Friedmann had shown (1922) that the Universe will not be static anyway. After some debate, Einstein admitted his mistake and called the introduction of a cosmological constant "the greatest blunder of my life".

So, why did the Universe not collapse under the pull of gravity? Resolution is in awkward initial conditions called the Big Bang, where velocity in Eq. (17) is highly tuned to potential energy, leading to practically zero spatial curvature and to $\rho = \rho_c$. This implies enormous fine-tuning for the Universe to survive till present. Such fine-tuning is hard to accept, and a modification of classical cosmology was called for. We will see how modern inflationary cosmology solves the problem of initial conditions. Again, the resolution is in anti-gravity caused by negative pressure.

2.3 Matter content in the Universe

To solve Friedmann equations, Eq. (5)-(6), one has to specify the matter content of the Universe and the equation of state for each of the constituents. To fit current observations we need at least four components

- *Radiation* (relativistic degrees of freedom). Today this component consists of the photons and neutrino and gives negligible contribution into total energy density. However, it was major fraction at early times.
- *Baryonic matter*. Makes up the observable world today.
- *Dark matter*. Was not directly detected yet, but should be there. Constitutes major matter fraction today. Has rather long observational history and can be fitted within frameworks of modern particle physics nicely, at the price of "moderate" tuning of parameters to provide required fraction of matter.
- *Dark energy*. Looks like it also should be there. It provides the major fraction of the total energy density today. Was not anticipated and appears as a biggest surprise and challenge for particle physics, though conceptually it can be very simple, being just a "cosmological constant" or vacuum energy.

Equations of state. Each of these components have very simple equation of state, parameterized by a single constant w

$$w \equiv \frac{p}{\rho} \ . \tag{21}$$

With a constant w, solutions of the first law of thermodynamics, Eq. (7), are readily found

$$\rho(t) = a(t)^{-3(1+w)} \ \rho_0 \ , \tag{22}$$

where ρ_0 stands for the present day density. For example, for ordinary forms of matter we have

- Radiation: $w = \frac{1}{3}$ and $\rho = a^{-4} \ \rho_0$. Result can be understood as a simple consequence of entropy conservation, $aT = \text{const}$, since for radiation $\rho \propto T^4$.
- Matter: $w = 0$ and $\rho = a^{-3} \ \rho_0$. Result can be understood as a simple consequence of particle number conservation, $na^3 = \text{const}$ and $\rho = mn$, where m is particle mass.

For hypothetical matter, which may play the role of dark energy, w is negative

- Network of cosmic strings: $w = -\frac{1}{3}$ and $\rho = a^{-2} \ \rho_0$.
- Network of domain walls: $w = -\frac{2}{3}$ and $\rho = a^{-1} \ \rho_0$.

– Cosmological constant: $w = -1$ and $\rho = \rho_0$. Result can be understood as a consequence of the Lorentz invariance of a vacuum, which restricts T^ν_μ to be proportional to the Kronecker tensor, $T^\nu_\mu = V\,\delta^\nu_\mu$. Comparing with Eq. (4) we find $p = -\rho$, or $w = -1$.

Law of expansion. Friedmann equation (5) in a spatially flat Universe and with a single matter component, which energy density evolves according to Eq. (22), has the solution

$$a = (t/t_0)^{\frac{2}{3(1+w)}} \ . \tag{23}$$

In particular

– Radiation: $w = \frac{1}{3}$, $a = (t/t_0)^{1/2}$
– Matter: $w = 0$, $a = (t/t_0)^{2/3}$
– Cosmological constant: $w = -1$. This case is special, and $a = \mathrm{e}^{H_0 t}$.

2.4 Cosmological Parameters.

These are used to parameterize the Fiedmann equation and its solution $a(t)$. Let me first summarize the current knowledge of numerical values of those parameters which were introduced already; later in the course we will discuss how these values were deduced.

Cosmological parameters

Symbol & Definition	Description	Present value
t	Age of the Universe	$t_0 = (13.7 \pm 0.2)$ Gyr
$H = \dot{a}/a$	Hubble constant	$H_0 = 71\ \mathrm{km\,s^{-1}\,Mpc^{-1}}$
$\rho_c = 3H^2/8\pi G$	Critical density	$\rho_c = 10\ h^2\ \mathrm{GeV\,m^{-3}}$
$\Omega = \rho/\rho_c$	Omega	$\Omega_0 = 1.02 \pm 0.02$
$\Omega_{\mathrm{CMB}} = \rho_{\mathrm{CMB}}/\rho_c$	Fraction of CMB photons	$\Omega_{\mathrm{CMB}} = 2.4 \cdot 10^{-5} h^{-2}$
$\Omega_b = \rho_b/\rho_c$	Baryonic fraction	$\Omega_b = 0.044 \pm 0.004$
$\Omega_m = \rho_m/\rho_c$	Matter fraction	$\Omega_m = 0.27 \pm 0.04$
$\Omega_\Lambda = \rho_\Lambda/\rho_c$	Dark Energy fraction	$\Omega_\Lambda = 0.73 \pm 0.04$

2.5 Cosmography.

We can define cosmography (this is my custom definition for these lectures) as a part of cosmology which tries to map observations into reconstruction of the scale factor. I.e., the goal is to find and tabulate the function $a(t)$. This is important in many respects: e.g. it allows to determine the matter content in the Universe (assuming the Friedmann equations are correct). One simple and straightforward way of tabulating the function is in determining its coefficients in Taylor expansion. This can be done making a Taylor decomposition around present time, $t = t_0$. The value of the scale factor at any moment of time can be fixed arbitrarily, we can use this freedom to choose $a(t_0) = 1$. The second term in the Tailor decomposition is naturally the value of the Hubble constant, H_0, Eq. (19). It gives us the rate of the Universe expansion at present and can be measured using the Hubble law, Eq. (20). One can go further in this decomposition and define the second derivative of the universe at present, the "deceleration parameter", and so on. We will not do it (at least at this point), since modern observations probe the whole function $a(t)$. Therefore, let us start with the preparation of the necessary machinery which allows us to deduce $a(t)$ from observations.

Let me stress now that Eq. (20) involves some degree of cheating since it is not a relation between the observables. (However, it is a valid relation for small separations.) To apply the Hubble law to observations, we have to derive its generalization, which would connect quantities we can measure.

Redshift. Looking at distant objects we see only the light they emit. How can physical quantities like distance and velocity be derived? Recall how a police officer determines the speed of a car. A similar principle is used in cosmology to determine the velocity of distant bodies. The shift of emission lines with respect to the frequency measurements by the local observer is related to velocity, and is used as an observable instead of the velocity. Systematic recession of objects, or cosmological expansion, leads to redshift. Note that cosmological redshift is not entirely due to the Doppler effect, but, rather, can be interpreted as a mixture of the Doppler effect and of the gravitational redshift.

Let us relate now the redshift to cosmological expansion, $\dot{a}/a$. To this end, we consider photon trajectories in a cosmological background with metric Eq. (2). The trajectory is given by $ds^2 = 0$. Since the overall scale factor does not change the solutions of $ds^2 = 0$, it is convenient to introduce the conformal time η defined as

$$dt = a(\eta)\, d\eta \ . \tag{24}$$

It is sufficient to consider radial trajectories with the observer at the center, and I restrict myself to a spatially flat metric $ds^2 = a^2(d\eta^2 - d\chi^2) = 0$, where χ denotes the radial coordinate. The solution of $d\eta^2 - d\chi^2 = 0$ is $\chi = \pm\eta + \text{const}$. Since the comoving distance between source and observer does not change, the conformal time interval between two light pulses is the same at the point of emission and at the point of observation, $\Delta\eta = \text{const}$. Using the definition of conformal time, $d\eta = dt/a$, we find

$$\frac{\Delta t}{a}|_{\text{emission}} = \frac{\Delta t}{a}|_{\text{detection}} \ .$$

Therefore, for a signal frequency we get $\omega_d a_d = \omega_e a_e$. Defining (measurable) redshift as

$$z \equiv \frac{\omega_e - \omega_d}{\omega_d} \tag{25}$$

we obtain

$$1 + z = \frac{a_d}{a_e} \ . \tag{26}$$

It is convenient to normalize the scale factor by the condition $a_d = 1$ at the point of detection, and to consider the scale factor at the point of emission as a function of redshift z. On the basis of this relation, the expansion history of the Universe can be parameterized as

$$a(z) = \frac{1}{1+z} \ . \tag{27}$$

The differential form of Eq. (27) is $da/dz = -a^2$. For future use, let us find now the relation between $d\eta$ and dz

$$d\eta \ = \ \frac{d\eta}{dt}\,\frac{dt}{da}\,\frac{da}{dz}\,dz \ = \ -\frac{a}{\dot{a}}\,dz \ = \ -\frac{dz}{H(z)} \ . \tag{28}$$

Observing that $d\eta = -d\chi$, we obtain the Hubble low for small separations, $dz = H d\chi$. At this point, we have succeeded in replacing the velocity by the redshift. Now we aim to relate the distance to some other quantity, directly measurable in cosmology.

Luminosity distance. Looking at distant objects we see only the light they emit. How can physical quantities like distance and velocity be derived? There are several ways to introduce a quantity related to the distance: different definitions are not equivalent in curved space-time. A definition based on flux measurements is the appropriate one, if "standard candles" can be found and used. Detected flux $[\text{erg s}^{-1}\,\text{sm}^{-2}]$ is inversely proportional to the distance from a source, $F \propto D^{-2}$. Namely, if L is intrinsic luminosity $[\text{erg s}^{-1}]$, we have

$$D_L^2 = \frac{L}{4\pi F} \ . \tag{29}$$

D_L is called the "luminosity distance". For this technique to work, one has to find a set of sources with a known or calibrated luminosity. If such can be defined, they are called *standard candles.*

To see how the luminosity distance enters the Hubble law, let us consider a space-time with the metric $ds^2 = a^2\ (d\eta^2 - d\chi^2 - \chi^2\ d\Omega)$. Now, go through the following list to find out what happens with the flux emitted into a frequency interval $d\nu$ by a source located at redshif z:

- Surface area at the point of detection is $4\pi\chi^2$. (Recall our choice $a_d = 1$).
- Energy and arrival rates are redshifted between the points of emission and detection. This reduces the flux by $(1+z)^2$.
- Opposing this tendency, the bandwidth $d\nu$ is reduced by $(1+z)$.
- Photons observed at a frequency ν, were emitted at $(1+z)\,\nu$.

Therefore, the measured spectral flux density is

$$S(\nu) = \frac{L((1+z)\,\nu)}{4\pi\,\chi^2(1+z)}\ . \tag{30}$$

For the bolometric flux (i.e. integrated over ν) we find

$$F = \frac{L}{4\pi\,\chi^2(1+z)^2}\ . \tag{31}$$

Comparing this with the definition, Eq. (29), we find for the luminosity distance

$$D_L = (1+z)\,\chi\ , \tag{32}$$

where χ is the comoving distance between the point of emission and the point of detection

$$\chi(z) = \int_{\eta_e}^{\eta_d} d\eta = \int_0^z \frac{dz'}{H(z')}\ . \tag{33}$$

In the last equality we have used Eq. (28). Therefore, the generalization of the Hubble law, which can be used in observational cosmology, can be written as

$$(1+z)\,\chi(z) = \sqrt{\frac{L}{4\pi F}}\ \ . \tag{34}$$

Parameterization of $\mathbf{H}(\mathbf{z})$. Let us express now the function $H(z)$ in the r.h.s. of Eq. (33) through the cosmological parameters. First, we define the ratio of the total energy density to the critical one

$$\Omega \equiv \frac{\rho_{\rm tot}}{\rho_c}\ . \tag{35}$$

The present day value is referred to as Ω_0. Similarly, for each energy component we denote its *present day* fractional contribution as $\Omega_i \equiv \rho_i/\rho_c$. With these definitions, the Friedmann equation (5) for a spatially flat Universe can be re-written as

$$H^2 = \frac{8\pi G}{3}\sum_i \rho_i\ ,$$

or

$$H^2 = H_0^2\ \sum_i \Omega_i\,(1+z)^{3(1+w_i)}\ . \tag{36}$$

Here I have used

$$\rho_i = \rho_{i,0}\ a^{-3(1+w_i)}\ = \rho_c\,\Omega_i\,(1+z)^{3(1+w_i)}\ ,$$

and expressed the scale factor as a function of redshift according to Eq. (26), and used the definition of the critical density, $H_0^2 = 8\pi G\rho_c/3$.

Parameterization (36) is ready for use in Eq. (33) for the comoving distance. In particular, this finalizes expression Eq. (34) for the luminosity distance.

3. Cosmic Microwave Background Radiation

The Universe is filled with radiation which is left-over from the Big Bang. The name for this first light is Cosmic Microwave Background Radiation (CMBR). Measurements of tiny fluctuations (anisotropy) in CMBR temperature give a wealth of cosmological information and became a most powerful probe of cosmology.

This radiation was predicted by Georgi Gamov in 1946, who estimated its temperature to be $\sim 5\ K^\circ$. Gamov was trying to understand the origin of chemical elements and their abundances. Most abundant, after hydrogen, is helium, with its shear being $\sim 25\%$. One possibility which Gamov considered was nucleo-synthesis of He out of H in stars. Dividing the total integrated luminosity of the stars by the energy released in one reaction, he estimated the number of produced He nuclei. This number was too small in comparison with observations. Gamov assumed then the oven where the light elements were cooked-up was the hot early Universe. He calculated abundances of elements successfully and found that the redshifted relic of thermal radiation left over from this hot early epoch should correspond to $\sim 5\ K^\circ$ at present. In one stroke G. Gamov founded two pillars (out of four) on which modern cosmology rests: CMBR and Big Bang Nucleosynthesis (BBN). Hot Big Bang was born.

Cosmic microwave background was accidentally discovered by Penzias and Wilson [15] at Bell Labs in 1965 as the excess antenna temperature which, within the limits of their observations, was isotropic, unpolarized, and free from seasonal variations. A possible explanation for the observed excess noise temperature was immediately given by Dicke, Peebles, Roll, and Wilkinson and was published in a companion letter in the same issue [16]. They were preparing dedicated search experiment, but were one month late. Penzias and Wilson measured the excess temperature as $\sim 3.5 \pm 1\ K^\circ$. It is interesting to note that the first (unrecognized) direct measurements of the CMB radiation was done by T. Shmaonov at Pulkovo in 1955, also as an excess noise while calibrating the RATAN antenna [17]. He published the temperature as $(3.7 \pm 3.7)\ K^\circ$. Prior to this, in 1940, Andrew McKellar [18] had observed the population of excited rotational states of CN molecules in interstellar absorption lines, concluding that it was consistent with being in thermal equilibrium with a temperature of $\approx 2.7\ K^\circ$. Its significance was unappreciated and the result essentially forgotten. Finally, before the discovery, in 1964 Doroshkevich and Novikov in an unnoticed paper emphasized [19] the detectability of a microwave blackbody as a basic test of Gamov's Hot Big Bang model. To me, as to theorist, the detection of CMBR looks nowadays like an easy problem. Indeed, a few percent of the "snow" on TV screens is due to CMBR.

The spectrum of CMBR is a perfect blackbody, with a temperature $T = 2.725 \pm 0.002\ K^\circ$ as measured by modern instruments. This corresponds to 410.4 photons per cubic centimeter or to the flux of 10 trillion photons per second per squared centimeter. The temperature is slightly different in different patches of the sky - to 1 part in 100,000. And this is most important: the spectrum of this tiny fluctuations tells us a lot about the fundamental properties of the Universe.

CMBR is the oldest light in the Universe. When registering it, we are looking directly at the deepest past we can, using photons. These photons had traveled the longest distances without being affected by scattering, and geometrically came out almost from the universe Horizon. More precisely, the CMB comes from the surface of the last scattering. We cannot see past this surface. That is because at early times the Universe was ionized and not transparent for radiation. With expansion, it cooled down, and when hydrogen recombined, the universe became transparent. Therefore the CMBR gives us a snapshot of the baby Universe at this time, which is called the time of last scattering. Let us determine when the last scattering had occurred in the early Universe.

3.1 Hydrogen recombination

At temperatures greater than a few thousands K, the ionized plasma in the Universe consisted of mostly protons, electrons, and photons, with a small fraction of helium nuclei and a tiny trace of some other light elements. To a good approximation we can consider only the hydrogen. Matter is then ionized at

temperatures higher than the hydrogen ionization energy $E_{\rm ion} = 13.6$ eV. At lower T neutral atoms start to form. The baryonic matter is in thermal equilibrium and the equilibrium fraction of ionized hydrogen can be described by the Saha equation (see Ref. [4] for more details)

$$\frac{n_e\, n_p}{n_{_H}} = \left(\frac{m_e T}{2\pi}\right)^{3/2} {\rm e}^{-E_{\rm ion}/T} \ , \tag{37}$$

here $n_e,\ n_p$ and $n_{_H}$ are the number densities of electrons, protons, and neutral hydrogen respectively. Plasma is electrically neutral, i.e. $n_e = n_p$. To find the closed relation for the fraction of ionized atoms, $X \equiv n_p/(n_p + n_{_H}) = n_p/n_{_B}$, we need the relation between the baryon number density, $n_{_B}$, and temperature. This relation can be parameterized with the help of an important cosmological parameter called *baryon asymmetry*

$$\eta = \frac{n_{_B}}{n_\gamma} = \frac{n_p + n_{_H}}{n_\gamma} = (6.1 \pm 0.3) \times 10^{-10} \ , \tag{38}$$

where n_γ is the number density of photons

$$n_\gamma = \frac{2\zeta(3)}{\pi^2} T^3 \ , \tag{39}$$

and $\zeta(3) = 1.202$, see Eq. (14). Baryon asymmetry can be estimated by an order of magnitude by simply counting the number of baryons, $\eta = 2.68 \times 10^{-8} \Omega_b h^2$. This is not the most precise method, though; the value presented in Eq. (38) was obtained from fitting the spectrum of CMBR fluctuations, see below. Nowadays, this is the most precise baryometer. Prior to this, the best estimates were obtained comparing BBN predictions of element abundances to observations. Defining recombination as the temperature when $X = 0.1$, we find $T_{\rm rec} \approx 0.3{\rm eV}$.

The Universe became transparent for radiation when the mean free path of photons became comparable to the size of the Universe at that time. Photons scatter mainly on electrons and we find that the Universe became transparent when

$$(\sigma_{\gamma e}\, n_e)^{-1} \ \sim \ t \ . \tag{40}$$

Here, $\sigma_{\gamma e} = 8\pi\alpha^2/3m_e^2$ is the Compton cross-section. For the temperature of last scattering we find $T_{\rm ls} \approx 0.26$ eV. Taking the ratio to the current CMBR temeperature we find $z_{\rm ls} \approx 1000$.

3.2 Spectrum is not distorted by red-shift

Prior to recombination photons were in thermal equilibrium. Therefore, at last scattering they have Planck spectrum

$$n(p) = \frac{1}{\exp(E_{\rm ls}/T_{\rm ls}) - 1} \ .$$

Since then, particle momenta are red-shifted, $p = k/a$. Since photons are massless, $E = p$, their energies are red-shifted at the same rate, $E_0 a_0 = E_{\rm ls} a_{\rm ls}$, and the spectrum becomes

$$n \ = \ \frac{1}{\exp(E_0/a_{\rm ls}T_{\rm ls}) - 1} = \frac{1}{\exp(E_0/T_0) - 1} \ ,$$

where we have used the notation $T_0 \equiv a_{\rm ls} T_{\rm ls}$. Therefore, after decoupling, the shape of the spectrum is not distorted. This statement would not be true for massive particles, $E^2 = (p/a)^2 + m^2$.

Measuring CMBR, we should still see the Planckian spectrum, but with red-shifted temperature. Clearly, this conclusion is true not only for cosmological red-shift, but for the gravitational red-shifts as well. E.g., fluctuations in the gravitational potential at the last scattering surface should cause fluctuations in CMBR temperature, but do not distort the spectrum.

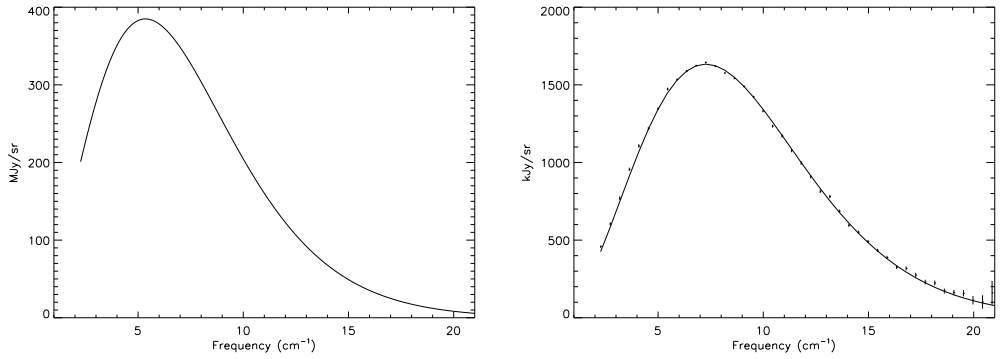

Fig. 3: Left panel: uniform spectrum; error-bars are a small fraction of the line thickness. Right panel: dipole spectrum; vertical lines indicate one σ uncertainties. From Ref. [20].

3.3 Dipole spectrum

Intensity of the CMB radiation is a function of the frequency $2\pi\nu = E$ and the direction on the sky (l, b). As a function of (l, b) it can be decomposed in spherical harmonics. Coefficients will be the functions of ν. The first two terms in this decomposition are

$$S(\nu, l, b) = I_0(\nu) + D(l, b)\, d(\nu) + \dots \ , \tag{41}$$

where $D(l, b) = \cos\theta$, and θ is an angle between observation and the maximum of the dipole $l_0 = 263.85^\circ$, $b_0 = 48.25^\circ$. The dipole is caused by our motion with respect to CMBR (which is composed of the motion of the Sun in the Galaxy and the Galaxy's own motion in the Local Cluster of galaxies). It gives the direction of this motion, l_0, b_0, which roughly coincides with the direction towards Virgo. The dipole induced by the velocity v is $vT\cos\theta$. This gives the magnitude of Sun's peculiar velocity, $(371 \pm 1)\ \mathrm{km\ s^{-1}}$.

Let $x \equiv E/T$. The monopole term should have the usual black-body spectrum $I_0(\nu) \propto x^3/(\mathrm{e}^x - 1)$. The dipole spectrum is actually distorted, because the Doppler frequency shift depends upon direction. The dipole spectrum can be found as a term linear in v in the Taylor decomposition of $S(\nu, l, b)$, with the result $d(\nu) \propto x^4\, \mathrm{e}^x\, /(\mathrm{e}^x - 1)^2$; for a recent discussion see Ref. [21]. Functions $I_0(\nu)$ and $d(\nu)$ are shown in Fig. 3, left and right panels respectively. Both agree with theoretical expectation.

3.4 Multipoles

Monopole and dipole contributions to CMBR, Eq. (41), can be subtracted. Emission of our Galaxy and various extragalactic sources can be subtracted also. This procedure uses the fact that the relic CMBR signal has a black body spectrum , which allows to distinguish it from other forms of radiation: measurements of the intensity at different frequencies allow to subtract contaminating foregrounds. What remains corresponds to the primordial cosmological pattern of temperature fluctuations, which is shown in Fig. 4. The upper panel presents the results of early COBE experiments [22], the lower panel shows the results of a recent WMAP experiment [9].

The temperature anisotropy, $T(\mathbf{n})$, as a function of viewing direction vector $\mathbf{n}$, is naturally expanded in a spherical harmonic basis, Y_{lm}

$$T(\mathbf{n}) = \sum_{l,m} a_{lm} Y_{lm}(\mathbf{n}) \ . \tag{42}$$

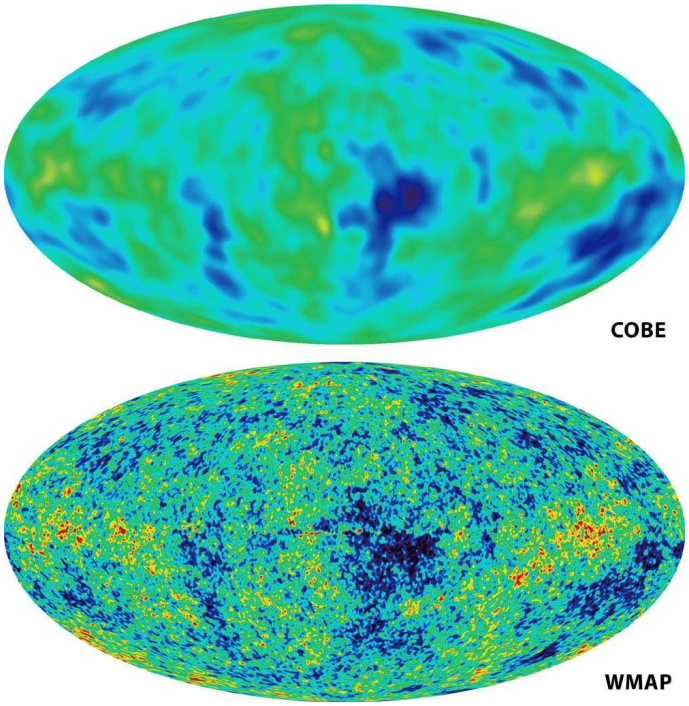

Fig. 4: Pattern of primordial temperature fluctuations in Galactic coordinates, from Ref. [9]. The WMAP map has 30 times finer resolution than the COBE map.

The coefficients in this decomposition, a_{lm}, define the angular power spectrum, C_l

$$C_l = \frac{1}{2l+1} \sum_m |a_{lm}|^2 \ . \tag{43}$$

The CMBR angular power spectrum as measured by WMAP experiment is shown in Fig. 5. The harmonic index l is related to the angular scale θ as $l \approx \pi/\theta$, so the first peak, at $l \approx 220$, would correspond to an angular scale of about one degree. Assuming random phases, the r.m.s. temperature fluctuation assosiated with the angular scale l can be found as

$$\Delta T_l = \sqrt{\frac{C_l \ l(l+1)}{2\pi}} \ . \tag{44}$$

Another representation of temperature fluctuations is given by the angular correlation function, which is related to C_l as

$$C(\theta) = \frac{1}{4\pi} \sum_l (2l+1) C_l \ P_l(cos \ \theta) \ , \tag{45}$$

where P_l is the Legendre polynomial of order l.

3.5 Tool of Precision Cosmology

The functional form of the CMBR power spectrum is very sensitive to both the various cosmological parameters and to the shape, strength and nature of primordial fluctuations. Measurements of the power spectrum provide us with a wealth of cosmological information at an unprecedented level of precision.

Right after the discovery of CMBR, it was realized that fluctuations in its temperature should have fundamental significance as a reflection of the seed perturbations which grew into galaxies and clusters. In a pure baryonic Universe it was expected that the level of fluctuations should be of the order

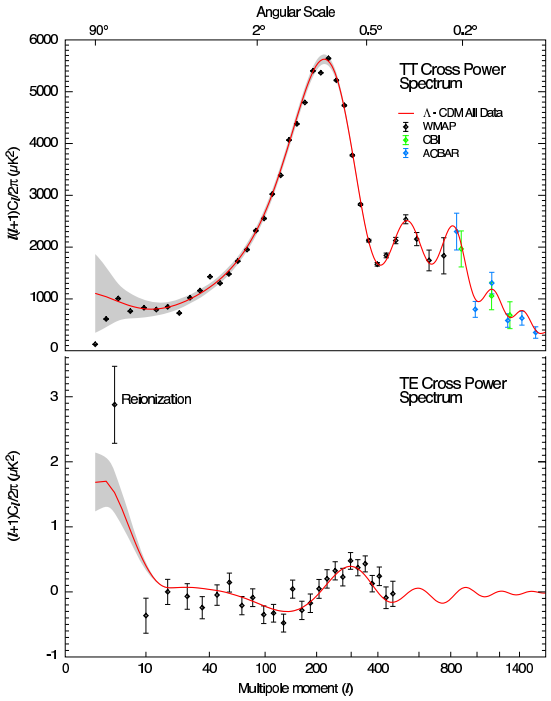

Fig. 5: The angular power spectrum of primordial CMBR temperature fluctuations is shown in the upper panel, from Ref. [9]. Black symbols ($l < 700$) are WMAP measurements, data points at smaller angular scales represent CBI and ACBAR experiments. Lower panel shows the temperature-polarization cross-power spectrum.

$\delta T/T \sim 10^{-2} - 10^{-3}$. Mesurements of the CMBR anisotropy with ever-increasing accuracy have begun. Once the temperature fluctuations were shown to be less than one part in a thousand, it became clear that baryonic density fluctuations did not have time to evolve into the nonlinear structures visible today. A gravitationally dominant dark matter component was invoked. Eventually, fluctuations were detected at the level of $\delta T/T \sim 10^{-5}$ [23], consistent with structure formation in Cold Dark Matter models with the Harrison-Zel'dovich spectrum of primordial perturbations motivated by cosmological inflation. Already this magnitude of $\delta T/T$ is very restrictive by itself. A partial set of best fit cosmological parameters, as derived from the recent measurments of CMBR anisotropies, is presented in Table I.

The foundations of the theory of CMBR anisotropy were set out by Sachs & Wolfe [24], Silk [25], Peebles & Yu [26], Syunyaev & Zel'Dovich [27]. The measured spectrum of CMBR power has a characteristic shape of multiple peaks. Positions of these peaks and their relative amplitudes are sensitive to many cosmological parameters in a non-trivial way. Fitting the data to model predictions gives very accurate values for many of these parameters (though there are some degeneracies between deferent sets). Numerical calculations for different models were done already in Ref. [28], and power spectra exhibiting acoustic peaks (similar to those in Fig. 5) were presented. It was realized, in particular, that positions of the peaks are shifted with respect to each other for adiabatic and isentropic primordial fluctuations.

3.6 Acoustic oscillations

Let us give a qualitative picture of why the CMBR power spectrum has a specific shape of a sequence of peaks, and explain how it depends on the values of particular cosmological parameters. Insight, sufficient for the purposes of these lectures, can be gained with the idealization of a perfect radiation fluid. In complete treatment, one has to follow the evolution of coupled radiation and metric fluctuations, i.e. to solve the linearized Einstein equations. However, essential physics of radiation (or matter) fluctuations

can be extracted without going into the tedious algebra of General Relativity. It is sufficient to consider the energy-momentum conservation, Eq. (8). To solve for metric perturbations, full treatment based on Einstein equations, Eq. (1), is needed of course. We will not do that here, but simply quote results for the evolution of the gravitational potentials (coincident in some important cases with the solutions for the Newtonian potentials).

Perturbations of the ideal radiation fluid, $p = \rho/3$, can be separated into perturbations of its temperature, velocity and gravitational potential. In the general-relativistic treatment gravitational potential appears as a fractional perturbation of the scale factor in the perturbed metric

$$ds^2 = a^2(\eta)\left[(1+2\Psi)d\eta^2 - (1-2\Phi)dx^i dx_j\right] . \tag{46}$$

Two equations contained in the energy-momentum conservation, $T^{\mu\nu}{}_{;\nu} = 0$ (i.e. temporal $\mu = 0$ and spatial $\mu = i$ parts of this equation), written in metric (46), can be combined to exclude the velocity perturbations. The resulting expression is simple

$$\ddot{\theta}_k + \frac{k^2}{3}\theta_k = -\frac{k^2}{3}\Phi_k + \ddot{\Phi}_k . \tag{47}$$

Note that this equation is the exact result for a pure radiation fluid. Here, θ_k are Fourier amplitudes of $\delta T/T$ with wavenumber k, and Φ_k is a Fourier transform of gravitational potential. Analysis of solutions of the Einstein equations for Φ shows that $\Phi_k = \mathrm{const}$ in two important cases:

1. For superhorizon scales, which are defined as $k\eta \ll 1$.
2. For all scales in the case of matter dominated expansion, $p = 0$.

In these situations the last term in the r.h.s. of Eq. (47), namely, $\ddot{\Phi}_k$, can be neglected. The Einstein equations also restrict the initial conditions for fluctuations. For the adiabatic mode in the limit $k\eta \ll 1$ one finds

$$\delta_i = -2\Phi_i , \tag{48}$$

where $\delta_i \equiv \delta\rho/\rho$. The adiabatic mode is defined as a perturbation in the total energy density. For the one component fluid, which we consider here, only the adiabatic mode can exist. Note that fractional perturbation of the scale factor in metric (46), $a(\eta, \mathbf{x}) = a(\eta) + \delta a(\eta, \mathbf{x}) \equiv a(\eta)(1 - \Phi)$, can be expressed as perturbation of spatial curvature, see Eq. (3). Therefore, adiabatic perturbations are also called curvature perturbations. Let us re-write Eq. (48) for temperature perturbations:

- Radiation domination, $\delta = 4\,\delta T/T$, and we find

$$\theta_i = -\frac{\Phi_i}{2} . \tag{49}$$

- Matter domination, $\delta = 3\,\delta T/T$, and we find

$$\theta_i = -\frac{2\Phi_i}{3} . \tag{50}$$

Recall now that in the limit $k\eta \ll 1$ the gravitational potentail is time-independent, $\Phi = \mathrm{const}$. Therefore, Eq. (47) has to be supplemented by the following initial conditions in the case of the adiabatic mode:

$$\theta_i \neq 0, \qquad \dot{\theta}_i = 0 . \tag{51}$$

Temperature fluctuations on largest scales. Let us consider the modes which had entered the horizon after matter-radiation equality, $k\eta_{\rm eq} < 1$. For those modes, $\dot{\Phi} = 0$ all the way from initial moments till present, and the solutions of Eq. (47) with adiabatic inital conditions is

$$\theta(\eta) + \Phi = (\theta_i + \Phi)\,\cos\left(\frac{k\eta}{\sqrt{3}}\right) . \tag{52}$$

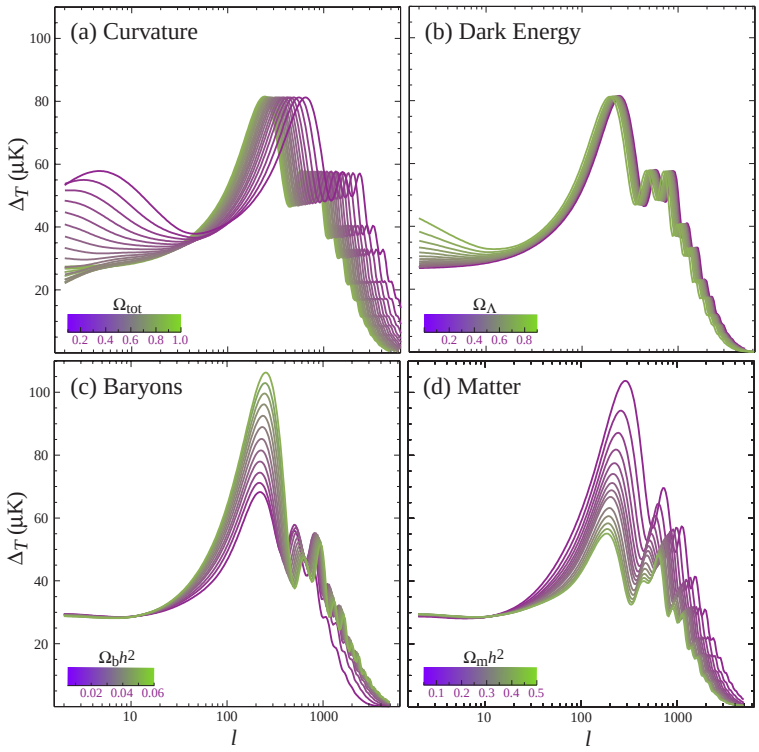

Fig. 6: Sensitivity of the CMBR angular power spectrum to four fundamental cosmological parameters (a) the curvature as quantified by $\Omega_{\rm tot}$ (b) the dark energy as quantified by the cosmological constant Ω_Λ ($w_\Lambda = -1$) (c) the physical baryon density $\Omega_b h^2$ (d) the physical matter density $\Omega_m h^2$, all varied around a fiducial model of $\Omega_{\rm tot} = 1$, $\Omega_\Lambda = 0.65$, $\Omega_b h^2 = 0.02$, $\Omega_m h^2 = 0.147$. From Ref. [29].

As gravity tries to compress the fluid, radiation pressure resists resulting in acoustic oscillations. It is important that oscillations are synchronized. All modes have the same phase regardless of k. This is a consequence of $\dot{\theta}_i = 0$, which is valid for all k. At the last scattering, the universe becomes transparent for the radiation and we see a snapshot of these oscillations at $\eta = \eta_{\rm ls}$.

To get its way to the observer, the radiation has to climb out of the gravitational wells, Φ, which are formed at the last scattering surface. Therefore the observed temperature fluctuations are $\theta_{\rm obs} = \theta(\eta_{\rm ls}) + \Phi$, or

$$\theta_{\rm obs} = \frac{1}{3}\Phi_i \cos\left(\frac{k\eta_{\rm ls}}{\sqrt{3}}\right) , \tag{53}$$

where we have used Eq. (50), which relates initial values of θ and Φ. Note that overdense regions correspond to cold spots in the temperature map on the sky, since the gravitational potential is negative. This is the famous Sachs-Wolfe effect [24].

Acoustic peaks in CMBR. Modes caught in the extrema of their oscillation, $k_n\eta_{\rm ls}/\sqrt{3} = n\pi$, will have enhanced fluctuations, yielding a fundamental scale, or frequency, related to the universe sound horizon, $s_* \equiv \eta_{\rm ls}/\sqrt{3}$. By using a simple geometrical projection, this becomes an angular scale on the observed sky. In a spatially flat Universe, the position of the first peak corresponds to $l_1 \approx 200$, see below. Both minima and maxima of the cosine in Eq. (53) give peaks in the CMBR power spectrum, which follow a harmonic relationship, $k_n = n\pi/s_*$, see Fig. 5.

The amplitudes of the acoustic peaks are recovered correctly after the following effects are taken into account: 1) baryon loading; 2) time-dependence of Φ after horizon crossing in radiation dominated

universe; 3) dissipation.

The effect of baryons is exactly the same for the oscillator equation Eq. (52), as if we had increased the mass of a load connected to a spring and oscillating in a constant gravitational field starting on top of an uncompressed coil at rest. The addition of baryons makes a deeper compressional phase, and therefore increases every other peak in the CMBR power spectrum. (First, third, fifth, ...) The CMBR power spectrum is a precise baryometer.

Gravitational potentials are not constant, but decay inside the horizon during radiation domination. This decay drives the oscillations: it is timed to leave compressed fluid with no gravitational force to fight when the fluid turns around. Therefore, the amplitudes of the acoustic peaks increase as the cold dark matter fraction decreases, which allows to measure Ω_m.

Dissipation leads to dumping of higher order peaks in the CMBR power spectrum.

The dependence of the CMBR angular power spectrum on different cosmological parameters is shown in Fig. 6.

Position of the first peak. Position of the first peak is determined by the angular size of the sound horizon at last scattering. Let us calculate here a similar quantity: the causal horizon (which is larger by a factor of $\sqrt{3}$ in comparison with the sound horizon). The comoving distance traveled by light, $ds^2 = 0$, from the "Big Bang" to redshift z is determined by a relation similar to Eq. (33), but with different integration limits

$$\eta(z) = \int_z^\infty \frac{dz'}{H(z')} \,, \tag{54}$$

where $H(z)$ is given by Eq. (36). One has to integrate this relation with a complete set of Ω_i, but for simplicity let us consider here the Universe dominated by a single component ρ_j

$$\eta(z) = \frac{(1+z)^{-\gamma_j}}{\gamma_j \, H_0} \,,$$

where $\gamma_j \equiv (1+3w_j)/2$. From the last scattering to $z \sim 1$, the Universe was matter dominated. Therefore, the causal horizon in matter dominated Universe $(w_j = 0)$

$$\eta(z) = \frac{2}{H_0\sqrt{1+z}}$$

should give a reasonable first approximation.

Consider two light rays registered at $z = 0$ which were separated by a comoving distance $\chi = \eta(z)$ at the moment of emission. Since both propagate in the metric $ds^2 = a^2(d\eta^2 - d\chi^2 - \chi^2 d\theta^2) = 0$, we find for the angular size of horizon at last scattering

$$\theta_h = \frac{\eta(z_{\rm ls})}{\eta(0)} = \frac{1}{\sqrt{1+z_{\rm ls}}} = \sqrt{\frac{T_0}{T_{\rm ls}}} \approx 2^\circ \,. \tag{55}$$

- This gives the position of the first acoustic peak, $l \approx 200$.
- Tells us that there were 10^4 causally disconnected regions at the surface of last scattering.

Horizon problem. Regions separated by more than $> 2^\circ$ have not been in the causal contact prior to the last scattering in the standard Friedmann cosmology. The microwave sky should not be homogeneous on scales $> 2^\circ$. Yet, CMB is isotropic to better than 10^{-4} on all scales. Observations tell us that all modes were, indeed, synchronized according to adiabatic initial conditions, Eq. (51), with only small initial perturbations present, $\Phi_i \ll 1$. This constitutes the so-called "Horizon problem" of standard cosmology. In Section 7. we will see how this problem is solved in frameworks of inflationary cosmology.

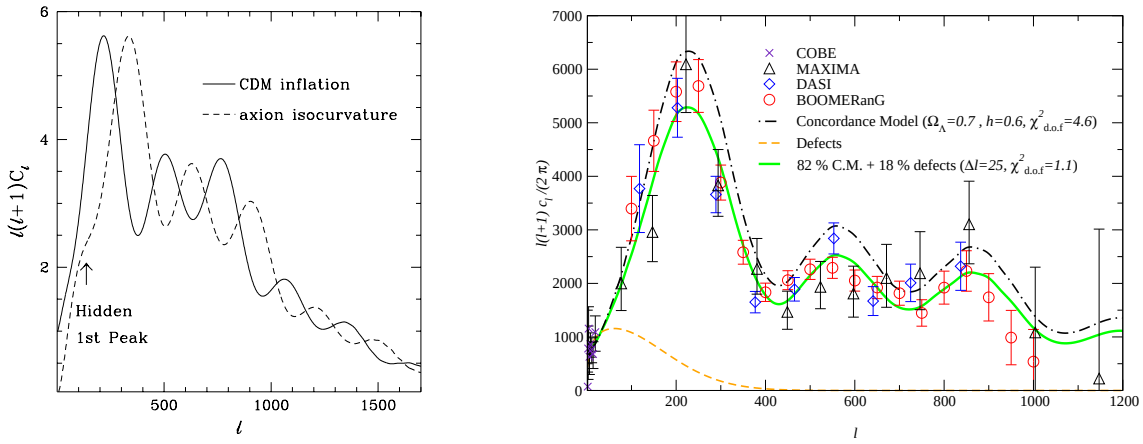

Fig. 7: Left panel: comparison of CMB power spectra in the models with adiabatic and isocurvature initial perturbations, from Ref. [30]. Right panel: adiabatic power spectra in comparison with spectra appearing in models seeded by topological defects, from Ref. [31]. In this panel some older, pre-WMAP, data are also shown.

Non-adiabatic perturbations. For the isocurvature perturbations, instead of Eq. (51), the initial conditions are given by

$$\delta_i = 0, \qquad \dot{\delta}_i \neq 0\ . \tag{56}$$

That is because, in this case, perturbation in total density (and therefore in curvature) are zero initially. As a consequence, in Eq. (52) we will have sine instead of cosine. Acoustic peaks will be shifted by half a period, see Fig. 7. Therefore, isocurvature perturbations are ruled out by modern CMBR experiments.

If density perturbations would be seeded by topological defects (e.g. cosmic strings), both sine and cosine will be present in the solution for temperature fluctuations, Eq. (52). That is because the source for Φ_k is active inside the horizon and phases of θ_k will be random. Acoustic peaks will be absent, see Fig. 7. Structure formation seeded primarily by topological defects is ruled out by modern CMBR experiments.

4. Large scale distribution of galaxies

Primordial cosmological fluctuations leave their imprint as CMBR anisotropies (discussed in the previous Section), and as density perturbations which give rise to galaxies and clusters of galaxies. CMBR anisotropies are observed on a two dimensional surface of last scattering, and therefore are measured as a two dimensional power spectrum. On the other hand, the distribution of galaxies can be measured in three dimensions. (Two angular coordinates of the line of sight to a galaxy and its redshift.) Different physical processes influence the initial perturbations until they are transformed into CMBR fluctuations or fluctuations of the distribution of galaxies. This influence can be encoded as a function of momenta, the transfer function $T(k)$, which simply maps the power spectrum of the initial perturbations into the observed power spectrum, and is a function of cosmological parameters. Therefore, the distribution of galaxies gives complimentary information with respect to CMBR anisotropies and helps to break degeneracy between cosmological parameters and the initial spectrum.

This is illustrated in Fig. 8 with CMBR data from WMAP and large-scale structure data from SDSS. The left panel corresponds to 95% constraints in the (Ω_m, h) plane. The shaded dark red region is ruled out by WMAP alone leaving the long banana region. This shows that these two basic cosmological parameters are not well constrained by WMAP alone. The shaded light red region is ruled out when SDSS information is added. The small (shown as white) region remain allowed. Note that the allowed region is in good agreement with a completely independent measurement by HST key project based on

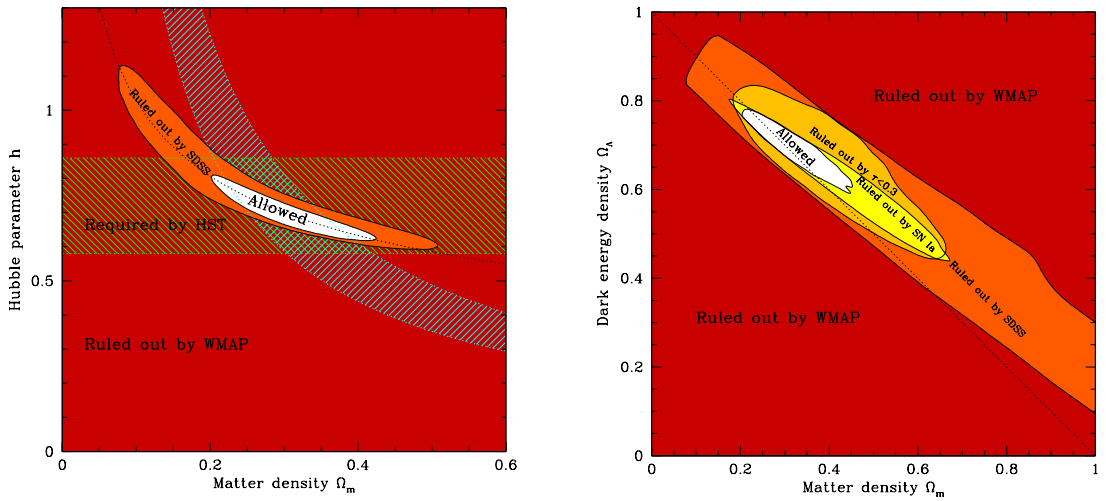

Fig. 8: Combined CMBR and large-scale structure constraints. **Left panel:** 95% constraints in the (Ω_m, h) plane. **Right panel:** 95% constraints in the $(\Omega_m, \Omega_\Lambda)$ plane. From Ref. [10].

entirely different physics. The combined WMAP + SDSS constraint is even tighter than HST project measurement.

One should bear in mind that there are caveats here. In deriving the WMAP+SDSS constraints which are shown in this figure, it was assumed that the universe is spatially flat, neutrino have negligible masses and the primordial spectrum is a pure power law. Without these priors the constraints are less tight.

The constraints in the $(\Omega_m, \Omega_\Lambda)$ plane with the assumption about spatial curvature being relaxed is shown in Fig. 8, right panel. The shaded dark red region is ruled out by WMAP alone, illustrating the well-known geometric degeneracy between models that all have the same acoustic peak locations. The shaded light red region is ruled out when adding SDSS information. Continuing inwards, the next two regions are ruled out allowing the assumption that re-ionization optical depth $\tau < 0.3$ and when supernova SN Ia information is included. $\Omega_\Lambda > 0$ is required with high confidence only when CMBR is combined with galaxy clustering information, or SN Ia information, see the next Section.

5. Dark energy

Something which is often called "Dark Energy" reveals itself in a variety of cosmological and astrophysical observations. This form of matter gravitates, but does not cluster. Contrary to radiation or dark matter, the dark energy causes the *accelerated* expansion of the universe. The need for it was hinted long ago to resolve conflict between the measured Hubble constant and the lower limits on the age of the Universe. Without the cosmological constant it was also not possible to obtain the correct growth of large scale structures in the $\Omega = 1$ Universe. Recently, the presence of dark energy was derived from the spectrum CMBR anisotropies and directly detected in the Hubble diagram of high redshift supernovae.

Age of the Universe. If there is no dark energy, the Universe should be matter dominated and should expand according to $a = (t/t_0)^{2/3}$. Differentiating this expansion law we find

$$Ht = 2/3\ . \tag{57}$$

The value of the Hubble constant, as derived by the Hubble Key Project from the Hubble diagram, is 72 ± 8 km s^{-1} Mpc^{-1} [14], see Fig. 2. On the other hand, the lower bound on the age of the Universe

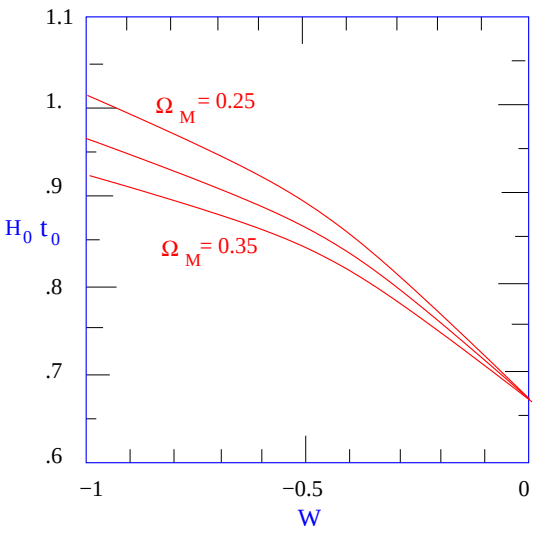

Fig. 9: Graphical representation of Eq. (61) assuming critical density, $\Omega_{\rm tot} = 1$.

can be established estimating the ages of various objects it consists of. For example, the temperature of the coldest white dwarfs in globular clusters yields a cluster age of 12.7 ± 0.7 Gyr [13]. This gives

$$H_0 t_0 > 0.93 \pm 0.12 \ , \tag{58}$$

in clear disagreement with Eq. (58). In other words, the Universe appears much younger than the ages of the oldest objects in it. The critical density Universe, $\Omega = 1$, cannot consist of pressureless matter if measurements of the Hubble constant are correct and Friedmann equations are valid.

The simplest cure (but "embarrassing" from the point of view of the particle physicist), is to add a cosmological constant, or dark energy. It should be stressed that this minimal modification of Friedmann equations is consistent with all other current cosmological tests and measurements. In the general case, the age of the Universe can be related to the expansion history as

$$t_0 = \int_0^{t_0} dt = \int_0^{t_0} a d\eta = \int_0^{\infty} \frac{dz}{(1+z)H(z)} \ . \tag{59}$$

Here we have used Eqs. (24), (27), (28). For two components, pressureless matter and dark energy with equations of state w, this relation can be written as (see Eq. (36)):

$$H_0 t_0 = \int_0^{\infty} \frac{dz}{(1+z)^{5/2}\sqrt{\Omega_M + \Omega_{\rm DE}(1+z)^{3w}}} \ . \tag{60}$$

The product $H_0 t_0$ as a function of w, assuming $\Omega_M + \Omega_{\rm DE} = 1$, is shown in Fig. 9. We see that it matches the observational constraints when $w \approx -1$ and $\Omega_M \approx 0.3$.

A discussion of further evidence for dark energy, e.g., related to the problem of the growth of density perturbations, can be found in Ref. [32].

Redshift - Luminosity Distance relation for Supernovae Ia. For the two-component energy content of the Universe, presureless matter and dark energy, the expression for the luminosity distance, Eq. (33), takes the form

$$D_L = \frac{1+z}{H_0} \int_0^z \frac{dz'}{(1+z')^{3/2}\sqrt{\Omega_M + \Omega_{\rm DE}(1+z')^{3w}}} \ , \tag{61}$$

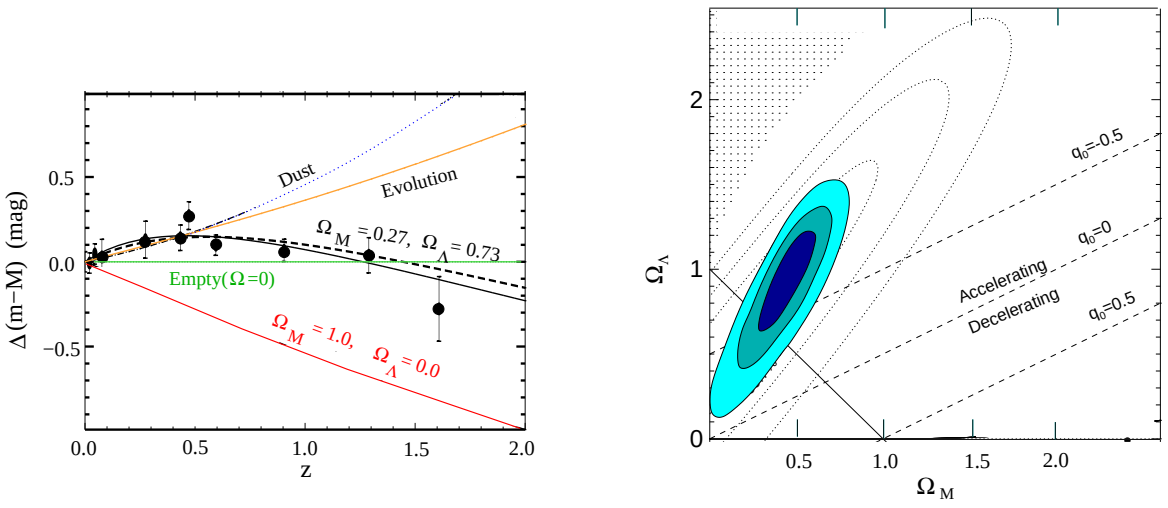

Fig. 10: **Left panel:** SN Ia residual Hubble diagram comparing astrophysical models and models for astrophysical dimming. Data (weighted averages in fixed redshift bins) and models are shown relative to an empty Universe model ($\Omega = 0$), adopted from Ref. [11]. **Right panel:** Joint confidence intervals for (Ω_M,Ω_Λ) from SNe Ia, Ref [11]. The dotted contours are the results from Ref. [33], illustrating the earlier evidence for $\Omega_\Lambda > 0$. The figure is adopted from Ref. [11].

see Eqs. (32), (33), (36). To use this relation as a cosmological test in conjunction with Eq. (34), one has to find a set of standard candles. This is a big challenge in practice, since we have to find very bright objects which can be seen from far away. At the same time, all of them should have the same luminosity, and we have to be sure that they do not evolve intrinsically. These requirements rule out galaxies and quasars. However, supernovae seem to be suitable. They are bright, as bright as the whole galaxy at the peak of luminosity, and Type Ia supernovae appear to be standard candles. These type of supernovae are thought to be nuclear explosions of white dwarfs in binary systems. The white dwarf, a stellar remnant supported by the degenerate pressure of electrons, accrete matter from a companion and its mass increases toward the Chandrasekhar limit of about $1.4\,M_\odot$. Near this limit, the degenerate electrons become relativistic, which leads to instability and the white dwarf explodes. This physics allows the explosions to be calibrated, since instability occur under the same conditions.

To proceed, I have to remark about the units of flux used by astronomers, which are magnitudes. The system is ancient, and has its origin in the logarithmic response of the human eye. The ratio of the flux of two objects is then given by a difference in magnitudes; i.e.,

$$m_2 - m_1 = -2.5 \log_{10}(F_2/F_1)\ . \tag{62}$$

A smaller magnitude means larger flux.

Fig. 10, left panel, shows the corresponding SNe Ia redshift-luminosity distance diagram. Data points correspond to magnitudes of SNe Ia measured at different redshifts. The case of $\Omega_M = 1$ (red curve) is ruled out. The "concordance model" $\Omega_M = 0.27$ and $\Omega_\Lambda = 0.73$ (black dashed curve) is within 1σ. For a flat geometry prior, best fit corresponds to $\Omega_M = 0.29 \pm^{0.05}_{0.03}$ (correspondingly $\Omega_\Lambda = 0.71$). Data are inconsistent with a simple model of evolution of SNe Ia, or dimming due to light absorption by dust as an alternatives to dark energy. The shaded area in Fig. 10, right panel, corresponds to 68%, 95% and 99.7% confidence levels in the (Ω_M, Ω_Λ) plane.

Constraints from CMB. Tight constraints on dark energy, and in a direction in parameter space which is "orthogonal" to SNe Ie constraints, are obtained from fitting the power spectrum of cosmic microwave background anisotropies, see the discussion in Section 3. The WMAP data alone rule out the standard

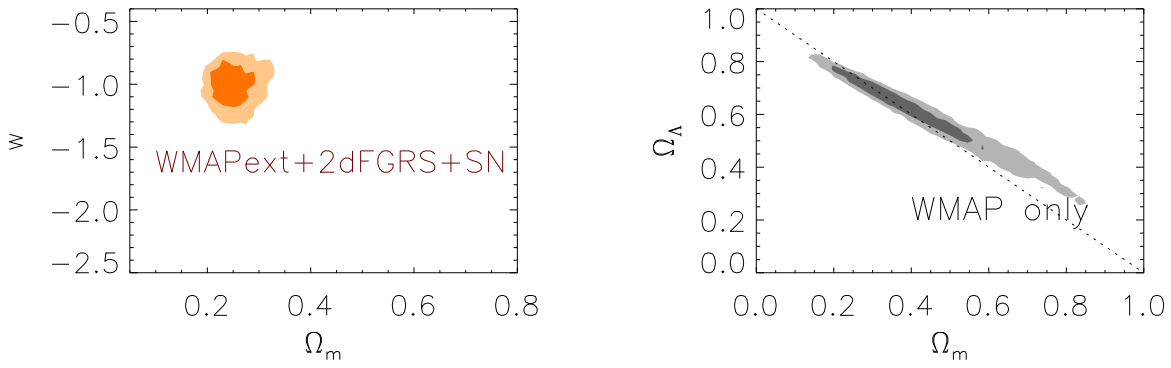

Fig. 11: **Left panel:** Constraints on the equation of state of dark energy in the (w, Ω_M) plane for a combination of the CMBR + 2dF + SNe Ia data sets. **Right panel:** Constraints on the geometry of the universe in the $(\Omega_M, \Omega_\Lambda)$ plane assuming the prior $h > 0.5$. From Ref. [34]

.

$\Omega_M = 1$ CDM model by 7σ if the prior $h > 0.5$ is accepted [9]. The resulting confidence levels in $(\Omega_M, \Omega_\Lambda)$ plane are shown in Fig. 11. While the CMBR data alone are compatible with a wide range of possible properties for the dark energy, the combination of the WMAP data with either the HST key project measurement of H_0, the 2dFGRS measurements of the galaxy power spectrum or the Type Ia supernova measurements requires that the dark energy be $\Omega_\Lambda = 0.73 \pm 0.04$ of the total density of the Universe, and that the equation of state of the dark energy satisfy $w < -078$ (95% CL) [9].

Constraints from gravitational lensing. Gravitational lensing will be discussed in Section 6.. Here we just note that the analysis of strong lensing of sources with known redshift is sensitive to the value of the geometrical cosmological parameters of the Universe. A recent study [35] of the lensing configuration in the cluster Abell 2218 is in agreement with the concordance model. In particular, assuming the flat Universe, it gives for the equation of state of dark energy $w < -0.85$. These constraints are consistent with the current constraints derived from CMB anisotropies or supernovae studies, but they are completely independent tests, providing nearly orthogonal constraints in the $(\Omega_M, \Omega_\Lambda)$ plane, see Fig. 18

Biggest Blinder – Biggest Surprise. From the point of view of the particle physicis,t the cosmological constant just should not be there. Indeed, in quantum field theory, the cosmological constant corresponds to vacuum energy, which is infinite and has to be renormalized,

$$\rho_{\rm vac} = \frac{1}{2\,(2\pi)^3} \int_0^{k_{\rm max}} \omega_k\, k^2\, dk \quad . \tag{63}$$

The natural value for the cut-off in this integral is the Plank scale, and then $\rho_{\rm vac} \sim M_{\rm Pl}^4 \approx 10^{74}$ GeV^4. Exact supersymmetry can make this integral vanish. Indeed, in Eq. (63), the contribution of one Bosonic degree of freedom is counted. Fermions contribute with an opposite sign, and if there is an equal number of Bosons and Fermions with equal masses, the vacuum energy will be zero. However, supersymmetry is broken at least at the electroweak scale, and then $\rho_{\rm vac}$ should not be smaller than $\sim M_{\rm W}^4 \approx 10^8$ GeV^4. Before dark energy was detected, it was believed that some yet unknown mechanism reduces the cosmological constant to zero. Zero is a natural number. However, it is hard to understand the smallness of the observed value $\rho_{\rm vac} \approx 10^{-46}$ GeV^4. Moreover, there is another pressing issue of fine tuning:

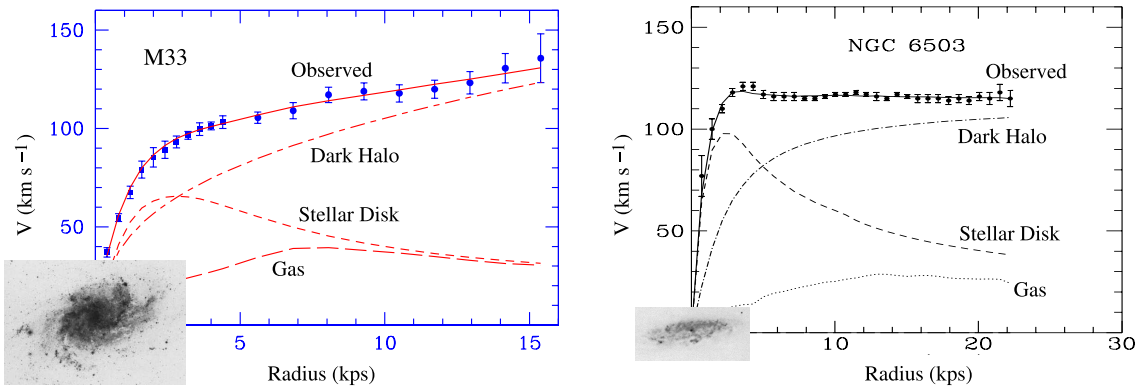

Fig. 12: The rotational curves of two sample galaxies. Left panel - M33, adapted from Ref. [36]. Right panel - NGC6503, adapted from Ref. [37]. I superimposed with the rotational curves the optical images of corresponding galaxies, approximately to scale.

why the detected value of $\rho_{\rm vac}$ approximately equals to the energy density of matter at the *present* epoch of cosmological evolution? The ratio of these two contributions scales as a^3 and, say, at recombination the vacuum energy was only 10^{-9} of matter energy... Detection of dark energy not only points to a new physics, but hints that we are missing SOMETHING very fundamental.

6. DARK MATTER

CMBR observations accurately measure the geometry of the Universe, its present expansion rate, its composition, and the nature and spectrum of the primordial fluctuations. Nevertheless, the traditional cosmological tests are still important. In particular, degeneracies between different parameter sets exist, which can produce the same CMBR spectra, and the conclusions drawn do rest upon a number of assumptions. Below we consider cosmological observations that are independent of the CMB and point to the existence of non-baryonic dark matter.

6.1 DARK MATTER: motivation

The missing mass is seen on all cosmological scales and reveals itself via:

- Flat rotational curves in galaxies.
- Gravitational potential which confines galaxies and hot gas in clusters.
- Gravitational lenses in clusters.
- Gravitational potential which allows structure formation from tiny primeval perturbations.

6.11 Dark Matter in Galaxies

Galactic rotational curves. Consider a test particle which is orbiting a body of mass M at a distance r. Within the frameworks of Newtonian dynamics the velocity of a particle is given by

$$v_{\rm rot} = \sqrt{\frac{G\,M(r)}{r}}\ . \tag{64}$$

Outside of the body, the mass does not depend on distance, and the rotational velocity should obey the Kepler law, $v_{\rm rot} \propto r^{-1/2}$. Planets of the Solar system obey this law. However, this is not the case

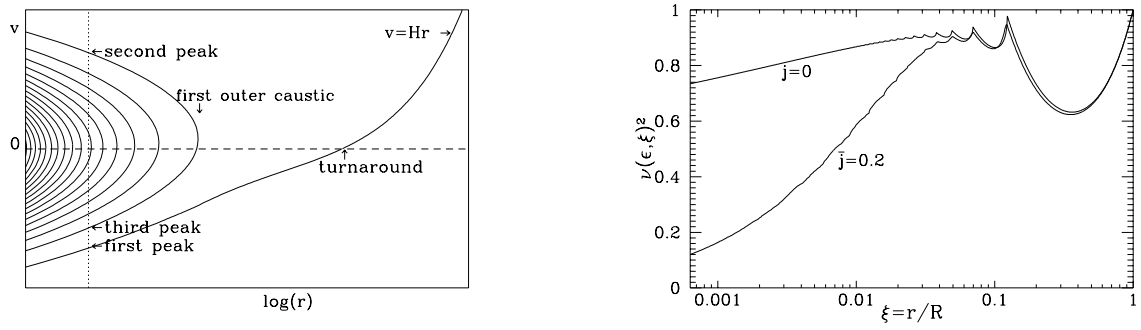

Fig. 13: Left panel: the phase space structure of an infall model. Right panel: rotational curves in an infall models. Two curves which correspond to different angular momenta are shown. From Ref. [40].

for stars or gas which are orbiting galaxies. Far away from the visible part of a galaxy, rotational curves are still rising or remain flat. Two examples are shown in Fig. 12. An optical image of the M33 galaxy is superimposed with its rotational curve, approximately to correct scale. The contribution of visible baryons in the form of stars and hot gas can be accounted for, and the expected rotational curve can be constructed. The corresponding contributions are shown in Fig. 12. One can see that the data-points are far above the contribution of visible matter. The contribution of missing dark mass, which should be added to cope with data, is also shown and is indicated as Dark halo. For the rotational velocity to remain flat, the mass in the halo should grow with the radius as $M(r) \propto r$, i.e., the density of dark matter in the halo should decrease as $\rho(r) \propto r^{-2}$.

Halo structure. For direct and indirect dark matter searches it is important to know the phase-space structure of the dark halo as well. With dark matter particles that are interactive, a thermal distribution over velocities would eventually be established. However, in conventional cold dark matter models, particles are non-interacting, except gravitationally. Binary gravitational interactions are negligible for elementary particles, and the resulting phase-space distributions are not unique, even for stationary equilibrium states, and even if flat rotational curves are reproduced.

1. The simplest self-gravitating stationary solution which gives flat rotational curves corresponds to an "isothermal sphere" with Maxwellian distribution of particles over velocities:

$$n(\vec{r}, \vec{v}) = n(r)\ e^{-v^2/v_0^2}\ . \tag{65}$$

Solution of the equation of hydrostatic equilibrium can be approximated by the density profile

$$\rho(r) = \frac{\rho_0}{(1+x^2)}, \quad \text{where } x \equiv r/r_c\ . \tag{66}$$

It should be stressed that the distribution Eq. (65), in contrast to a distribution in real thermal equilibrium, depends on particle velocities, not on their energies. Such distributions may arise in time-dependent gravitational potential as a result of collisionless relaxation.

2. There exist several density profiles which are empirical fits to numerical simulations, e.g. Navarro, Frenk & White (NFW) profile [38] and Moore *et al.* profile [39]

$$\rho(r) = \frac{\rho_0}{x\ (1+x)^2} \qquad \text{NFW}, \tag{67}$$

$$\rho(r) = \frac{\rho_0}{x^{3/2}\ (1+x^{3/2})} \qquad \text{Moore } et\ al. \tag{68}$$

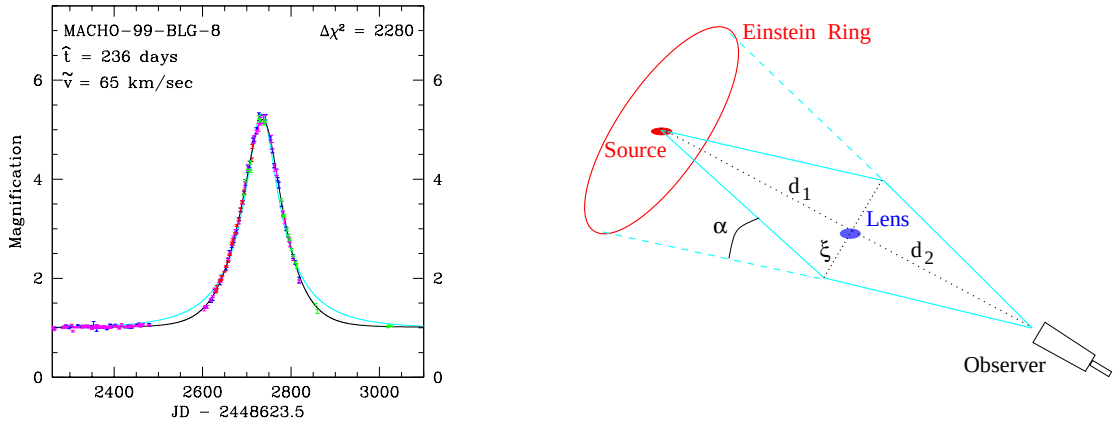

Fig. 14: Left panel: one of the detected microlensing effects, see Ref. [44]. Right panel: schematic view of gravitational lensing by point mass.

4. In the cold dark matter model, the distribution of particles in the phase space during initial linear stage prior to structure formation corresponds to thin hypersurface, $\mathbf{v} = H\mathbf{r}$ (or line in the Hubble diagram). Since during collisionless evolution the phase-space density conserves, at the non-linear stage the distribution will still be a thin hypersurface. If can be deformed in a complicated way and wrapped around, but it cannot tear apart, intersect its own folds, puff up or dissolve. The corresponding phase-space distribution for the case of spherical symmetry is shown in Fig. 13, left panel. With time, non-linear structure grows, and the infall of new particles continues. This manifests itself as a growth of turnaround radius (which is a surface where $v = 0$; the turnaround radius of our Galaxy is at 1 Mpc, see Ref. [41]) and as an increasing number of folds inside turnaround. The energy spectrum of dark matter particles at a fixed position will be discrete, see Fig. 13, left panel, where several velocity peaks are indicated at intersections of the vertical dashed line, $r = \mathrm{const}$, with phase-space sheets. The overall shape of the spectrum also changes compared to an isothermal distribution. This may be important for direct dark matter searches.

The infall model reproduces flat rotational curves, see Fig. 13, right panel. There is one interesting difference, though; rotational curves of the infall model have several small ripples in the region where the curve is flat. These ripples appear near the surfaces where $v = 0$. In principle, they may be detectable [42, 43] and then it will give a clear, unique signature of the presence of dark matter in galactic halo, (as opposed to models which try to explain apparent violation of Kepler's law by modification of gravity).

Existence of such a folded structure is a topological statement. However, in the inner halo the number of folds is very large, and limited resolution makes the distribution indistinguishable from, say, isothermal. It is not clear at which distances the description of halo in terms of the infall becomes appropriate. But for sufficiently isolated galaxy, in regions closer to the outer rim of the halo, where the number of folds is still small, signatures of the infall should exist, and they do exist in our Galaxy [41].

Baryonic Halo Dark Matter ? No. Already CMBR alone tells us that there should be non-baryonic dark matter, see Table I. BBN and CMB agree on $\Omega_B = 0.04$, however, contribution of stars amounts only to $\Omega_{\mathrm{stars}} = 0.005$. There should be dark baryons hiding somewhere. Can it be that the whole, or at least some part, of the halo dark matter is comprised of dark baryons in the form of non-luminous objects? Candidates are Jupiter like planets, brown dwarfs (which are undersized stars, too light to ignite thermonuclear reactions), or already dead stars (white dwarfs, neutron stars, or even black holes). This class of objects got the acronym MACHO, from MAssive Compact Halo Objects. Special techniques

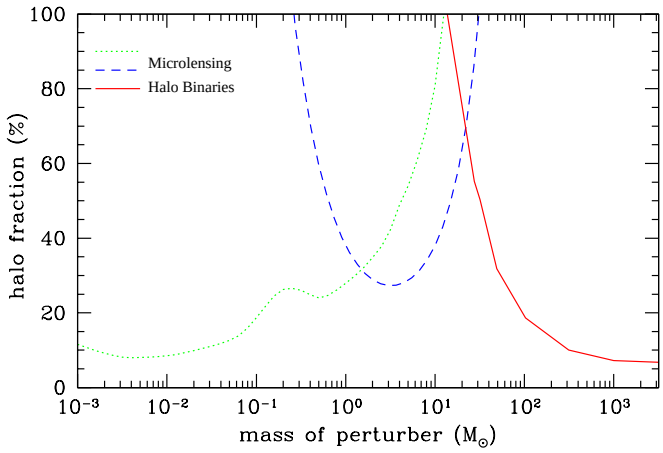

Fig. 15: 95% confidence limits on the MACHO fraction of the standard local halo density. Green and blue lines - results of EROS [45] and MACHO [46] microlensing collaborations. Red line - constraint from the absence of distortion of distribution of binary stars in angular separation [47]. Note that the microlensing exclusion curve extends outside of the plotted range and up to $M \sim 10^{-7} M_\odot$, see Ref. [45].

based on gravitational lensing were developed for MACHO searches. These searches were successful, but by now it is clear that MACHOs cannot comprise the whole dark matter, as their fraction of DM halo is restricted to be $< 50\%$. Since MACHOS are the only type of dark matter which has been detected, let us consider the issue in some more detail.

Consider the light deflection by a point mass M. If the impact parameter ξ is much larger than the Schwarzschild radius of the lens, $\xi \gg 2GM$, then General Relativity predicts that the deflection angle of a light ray, α, is

$$\alpha = \frac{4GM}{\xi} \,. \tag{69}$$

This is twice the value obtained in Newtonian gravity. If the lens happens to be on the line which connects the observer and a source, the image appears as a ring with the radius (Einstein ring radius)

$$r_E^2 = 4\,GM_L\,\frac{d_1 d_2}{d_1 + d_2} \,, \tag{70}$$

see Fig. 14, right panel. If the deflector is displaced from the line of sight by the distance r, then instead of the ring, an odd number of images will appear. If the images cannot be observed separately, because the resolution power of the telescope is not sufficient, then the only effect will be an apparent brightening of the source, an effect known as gravitational microlensing. The amplification factor is

$$A = \frac{2 + u^2}{u\sqrt{4 + u^2}} \,, \tag{71}$$

where $u = r/r_E$. If the lens is moving, the distance r will be changing with time, and the image of the background star will brighten during the closest approach to the line of sight. If the galactic halo is filled with MACHOs, this may happen occasionally for some of background stars. The typical duration of the light curve is the time it takes a MACHO to cross an Einstein radius, $\Delta t \sim r_E/v$, where $v \sim 10^{-3}$ is typical velocity in the halo. If the deflector mass is $1\,M_\odot$, the average microlensing time will be 3 months, for $10^{-2}\,M_\odot$ it is 9 days, for $10^{-4}\,M_\odot$ it is 1 day, and for $10^{-6}\,M_\odot$ it is 2 hours.

An optical depth for microlensing of the galactic halo is approximately $\tau \sim 10^{-6}$. Thus, if one looks simultaneously at several millions of stars during an extended period of time, one has a good

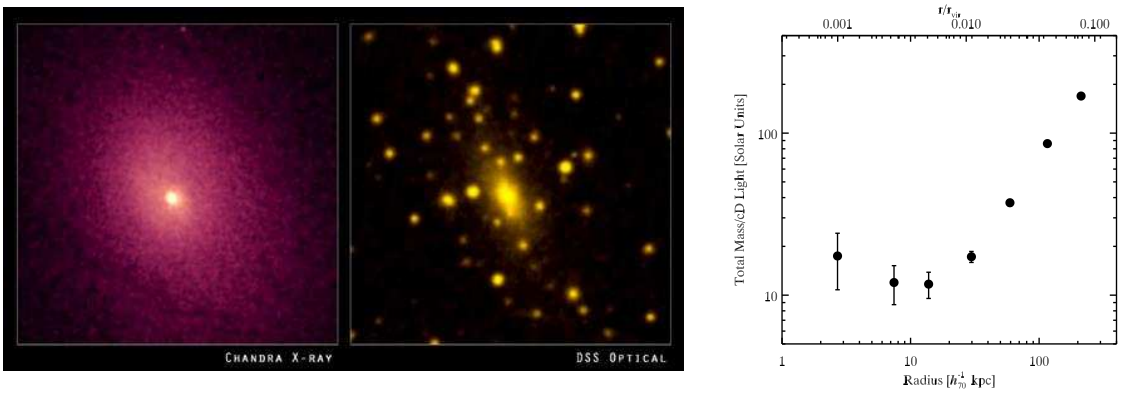

Fig. 16: X-ray (left panel) and optical (middle panel) images of the Abell 2029 cluster of galaxies. Right panel: ratio of total enclosed cluster mass to light in A2029, from Ref. [49].

chance of seeing at least a few of them brightened by a dark halo object. The first microlensing events were reported in 1993. Nowadays, there are more than half a hundred registered events. One of them is shown in Fig. 14. However, derived optical depth is not sufficient to account for all dark matter in the Galaxy halo. 95% confidence limits on the MACHO fraction of the standard local halo density is shown in Fig. 15.

Since MACHOs cannot account for the mass of the dark halo, non-baryonic dark matter should be present out there.

6.12 Dark Matter in Clusters of Galaxies

Already in 1933, F. Zwicky [48] deduced the existence of dark matter in the Coma cluster of galaxies. Nowadays, there are several ways to estimate masses of clusters, based on the kinetic motion of member galaxies, on X-ray data, and on gravitational lensing. These methods are different and independent. In the dynamical method, it is assumed that clusters are in virial equilibrium, and the virialized mass is easily computed from the velocity dispersion. In X-ray imaging of hot intracluster gas, mass estimates are obtained assuming hydrostatic equilibrium. Mass estimates based on lensing are free of any such assumptions. All methods give results which are consistent with each other, and tell that the mass of the luminous matter in clusters is much smaller than the total mass.

Kinetic mass estimates. Those are based on the virial theorem, $\langle E_{\rm pot}\rangle + 2\langle E_{\rm kin}\rangle = 0$. Here $\langle E_{\rm kin}\rangle = N\langle mv^2\rangle/2$ is averaged kinetic energy of a gravitationally bound object (e.g. cluster of N galaxies) and $\langle E_{\rm pot}\rangle = -N^2\langle m^2\rangle/2\langle r\rangle$ is its averaged potential energy. Measuring the velocity dispersion of galaxies in the clusters and its geometrical size gives an estimate of the total mass, $M \equiv N\langle m\rangle$.

$$M \sim \frac{2\langle r\rangle\langle v^2\rangle}{G} \; . \tag{72}$$

The result can be expressed as mass-to-light ratio, M/L, using the Solar value of this parameter. For the Coma cluster, which consists of about 1000 galaxies, Zwicky [48] has found

$$\frac{M}{L} \sim 300\, h\, \frac{M_\odot}{L_\odot} \; . \tag{73}$$

Modern techniques end up with very much the same answer. M/L ratios measured in Solar units in central regions of galaxies range from a few to 10 in spirals and large ellipticals. If clusters are large enough systems for their M/L to be representative of the entire Universe, one finds [50]

$$\Omega_M \approx 0.2 - 0.3 \; . \tag{74}$$

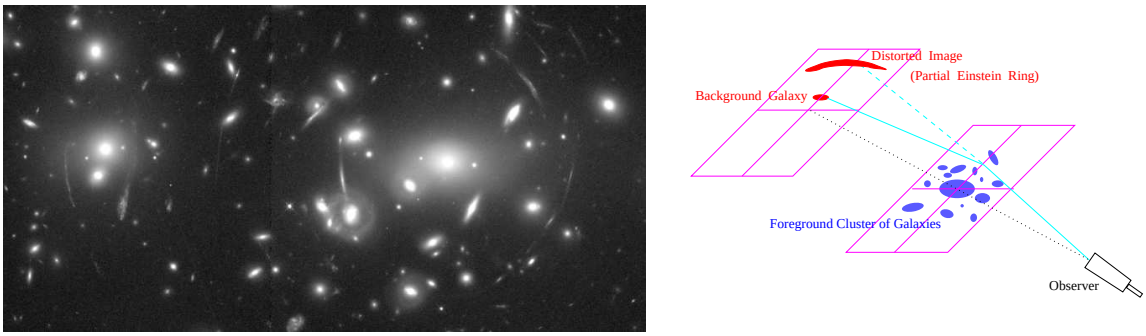

Fig. 17: Left panel: an image of the cluster Abell 2218 taken with the Hubble space telescope (see Ref. [52]). Spectacular arcs resulting from strong lensing of background galaxies are clearly seen.

Mass estimates based on X-rays. Mass is also traced in clusters of galaxies by hot gas which is visible in X-rays. Assume hot gas is in thermal equilibrium in a gravitational well created by a cluster. Then its density distribution $\rho_g(r)$ and pressure $P_g(r)$ satisfy

$$\frac{1}{\rho_g(r)}\frac{dP_g(r)}{dr} = -\frac{GM(\leq r)}{r^2} \ . \tag{75}$$

Observationally, the gas density follows from the X-ray luminosity. Gas temperature can be measured from the shape of X-ray spectrum. By measuring the temperature profile of a gas, one can reconstruct the gas pressure $P_g(r)$. In this way, the radial run of mass can be deduced.

For example, detailed modeling [49] of Abell 2029, which is shown in Fig. 16, leads to the conclusion that the cluster is dark matter dominated all the way into its core. After subtracting the contributions of stars and hot gas into the mass budget, the density profile of dark matter can be reconstructed. It agrees with NFW dark matter profile, Eq. (68), $\rho \propto 1/x(1+x^2)$, where $x \equiv r/r_s$ and $r_s = 540$ kpc. The agreement is remarkably good on all scales measured, 3 - 260 kpc. Baryons contribute $f_b \approx 14\%$ into the total mass of the cluster. Assuming universal baryon mass fraction and Ω_b from big bang nucleosynthesis, this also gives $\Omega_m \approx \Omega_m/f_b \approx 0.29$ for the total mass budget in the Universe, in agreement with other current estimates.

The same methods can be employed for studies of dark matter in large elliptical galaxies. In Ref. [51] the mass profile of the elliptical galaxy NGC 4636, based on the temperature of hot interstellar gas, was obtained for distances from 0.7 to 35 kpc. It was found that the total mass increases as radius to the power 1.2 over this range in radii, attaining a mass-to-light ratio of 40 solar masses per solar visual luminosity at 35 kpc. As much as 80% of the mass within the optical half-light radius is non-luminous in this galaxy.

Gravitational Lensing. Gravitational lensing allows direct mass measurement without any assumptions about the dynamical state of the cluster. The method relies on the measurement of the distortions that lensing induces in the images of background galaxies. As photons travel from a background galaxy to the observer, their trajectories are bent by mass distributions, see Fig. 17, right panel. Consider the deflection by a point mass M. For impact parameter ξ which is much larger than the Schwarzschild radius of the lens, $\xi \gg 2GM$, the deflection angle α is given by Eq. (69). If the gravitational field is weak, the deflection angle of an ensemble of point masses will be the vectorial sum of the deflections due to individual lenses.

A reconstruction of lens geometry provides a map of the mass distribution in the deflector. For a review of the method see e.g. Ref [53]. The images of extended sources are deformed by the gravitational field. In some cases, the distortion is strong enough to be recognized as arcs produced by galaxy clusters

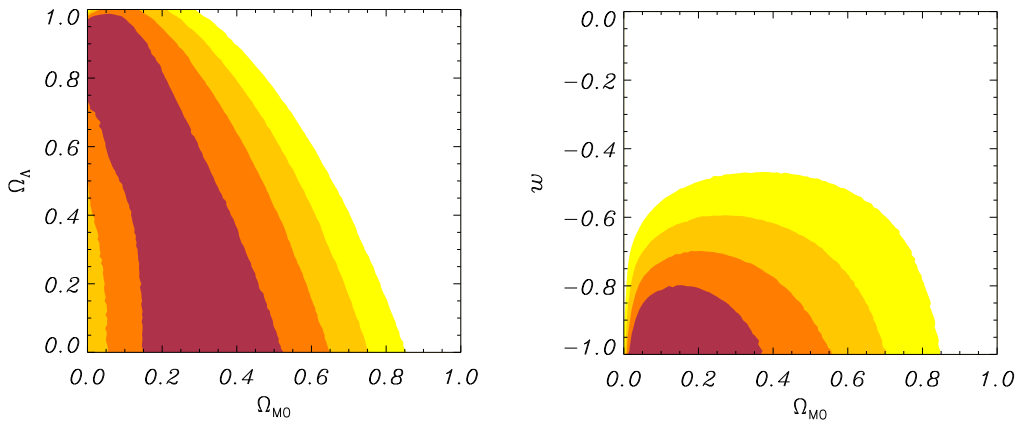

Fig. 18: The constraints on cosmological parameters obtained from the study of the lensing configuration in the Abell 2218 cluster of galaxies [35].

serving as a lens, see Fig. 17, left panel. For the cluster A 2218, shown in this figure, Squires et al. [54] compared the mass profiles derived from weak lensing data and the X-ray emission. The reconstructed mass map qualitatively agrees with the optical and X-ray light distributions. A mass-to-light ratio of $M/L = (440 \pm 80)h$ in solar units was found. Within the error bars the radial mass profile agrees with the mass distribution obtained from the X-ray analysis, with a slight indication that at large radii the lensing mass is larger than the mass inferred from X-rays. The gas to total mass ratio was found to be $M_{\rm gas}/M_{\rm tot} = (0.04 \pm 0.02)\, h^{-3/2}$.

Interestingly, the analysis of multiple images of several sources with known (and significantly different) redshift produced by a cluster lens is sensitive to the value of the geometrical cosmological parameters of the Universe. Study [35] of the lensing configuration in the cluster Abell 2218 gives $0 < \Omega_M < 0.30$ assuming a flat Universe, and $0 < \Omega_M < 0.33$ and $w < -0.85$ assuming flat Universe with dark energy, see Fig. 18. These constraints are consistent with the current constraints derived with CMB anisotropies or supernovae studies, however this method is a completely independent test, providing nearly orthogonal constraints in the $(\Omega_M, \Omega_\Lambda)$ plane.

6.2 Structure formation and DM

By present time the structure in the Universe (galaxies and clusters) is formed already, the perturbations in matter $\delta\rho/\rho \gtrsim 1$. However, the initial perturbations were small $\delta\rho/\rho \sim 10^{-5}$. Perturbations do not grow in the radiation dominated epoch, they can start growing only during matter domination $\delta\rho/\rho \sim a = 1/z$. Moreover, baryonic plasma is tightly coupled to radiation, therefore perturbations in baryonic matter start to grow only after recombination. For the same reason, initial perturbations in baryons at the time of recombination equal to fluctuations in CMBR. If baryons were to constitute the only matter content, then perturbations in matter at present time would be equal to

$$\frac{\delta\rho}{\rho}|_{\rm today} = z_{\rm rec}\, \frac{\delta\rho}{\rho}|_{\rm rec} \sim 10^{-2}\ , \tag{76}$$

where $z_{\rm rec} \approx 1100$ is the redshift of recombination. This is one of the strongest and simplest arguments in favour of non-baryonic dark matter. Structure has had time to develop only because perturbations in non-baryonic dark matter have started their growth prior to recombination. Baryonic matter then "catch up" simply by falling into already existing gravitational wells. If one aims to explain things by modification of gravity, one has to explain not only the flat rotational curves in galaxies and the presence of dark matter in galaxy clusters, but has also to provide the accelerated growth of structure from recombination till present, in a consistent way.

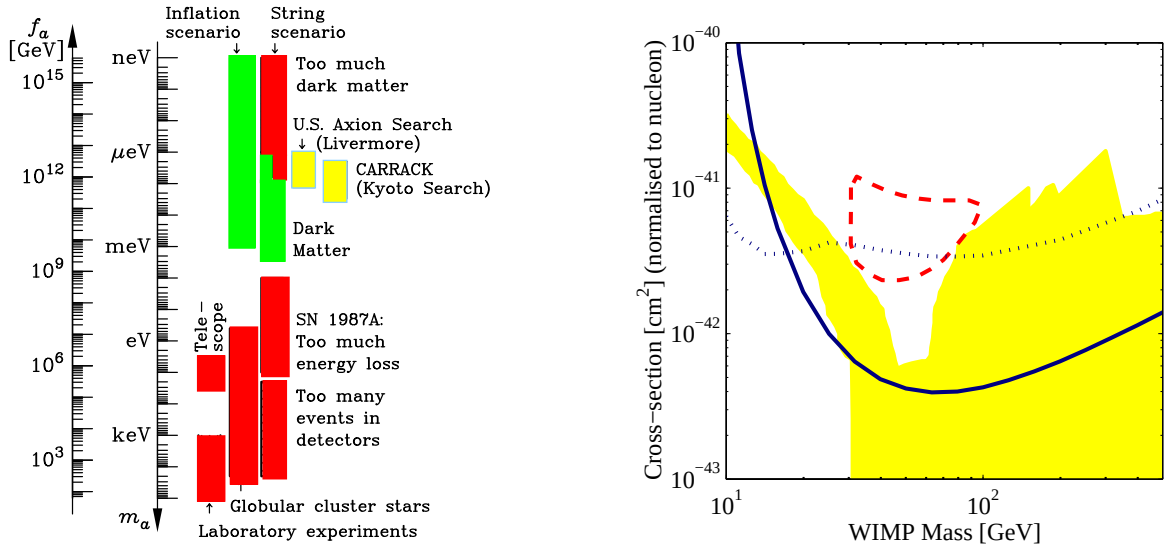

Fig. 19: **Left panel:** The constraints on axion parameters. Red blocks - various cosmological and astrophysical constraints; yellow blocks - exclusion regions obtained in dedicated dark matter search experiments; green blocks - the allowed regions in two cosmological scenarios. **Right panel:** Solid curve - the exclusion limits on the coherent WIMP-nucleon scalar cross-section obtained by CDMS collaboration in the direct dark matter search experiment; the parameter space above the curve is excluded at the 90% C.L. These limits are inconsistent with the DAMA 3σ signal region [73] (closed dashed contour) if it is due to scalar coherent WIMP interactions. Also shown are limits from CDMS at SUF (dotted line). The typical predictions of supersymmetric models are shown in yellow. Adapted from Ref. [74].

6.3 Non-baryonic Dark Matter Candidates

There is no lack for dark matter candidates in particle physics models. Some of them appear naturally, and were motivated by some other reasoning, not related to the dark matter problem. They are the leading candidates and are listed below.

- Axion. Has a mass $m \sim 10^{-5}$ eV. Appeared [55, 56] as a by-product of a suggested solution of the strong CP problem via a global $U(1)$ Peccei-Quinn symmetry [57]. The axion picks up a small mass in a way similar to the pion when chiral symmetry is broken. The parameters of these two particles are related, in particular $m_a \sim m_\pi f_\pi / f_a$, where f_a, is the axion decay constant, and determines also the strength of the axion coupling to other particles. There are tight astrophysical and cosmological bounds on f_a which leave only a narrow window, 10^{10} GeV $\lesssim f_a \lesssim 10^{12}$ GeV, see Fig. 19, the left panel. For the review of axion physics and searches see e.g. Refs. [58, 59].
- Neutrino, $m \sim 0.1$ eV. The only dark matter candidate which is known to exist. For this reason we discuss the neutrino in some more detail below. For the review of neutrino cosmology see e.g. Ref. [60], and for the neutrino astrophysics see e.g. Ref. [61]. While the neutrino is cosmologically important, it cannot resolve the dark matter problem.
- Mirror matter, $M \sim 1$ GeV. Does not belong to the list of the most popular candidates, but is attractive as an example of a model [62, 63, 64] where the approximate equality of baryonic and non-baryonic contributions into the energy balance of the Universe is attempted to be explained naturally, and not as a result of fine-tuning of model parameters.
- WIMP, $m \sim 100$ GeV. The most popular candidate, a natural outcome of supersymmetry. The lightest supersymmetric particle (or LSP) is naturally stable and would have interesting cosmological abundance. Known also under the names Neutrallino (dark matter has to be color and electrically neutral) and WIMP (from Weakly Interacting Massive Particle). For recent reviews see e.g. Refs. [65, 66]. The current status of direct and indirect WIMP searches is reviewed in

Ref. [67]. The new limits obtained by the CDMS collaboration and not reflected in cited reviews are shown in Fig. 19, the right panel.

- WIMPZILLA, $m \sim 10^{13}$ GeV. The newcomer, was initially motivated as a solution of the Greizen-Zatsepin-Kuzmin puzzle of Ultra-high energy cosmic rays [68, 69]. The popularity was boosted by the observation that cosmologically interesting abundance is created naturally, just as a sole consequence of Universe expansion [70, 71].

Non-baryonic dark matter model building and searches makes and extensive subject on its own. There are many dedicated excellent reviews, I cannot list them all, see e.g. some earlier [72] and the latest [65, 66, 67] one. For this reason, and because of space limitations, I will not describe non-baryonic dark matter in all its variety, instead I'll spend some time on simple and universal relations.

Cosmological density of neutrino. Here we calculate the abundance of particles which were once in thermal equilibrium with the rest of cosmological plasma. Let us first consider the case of the neutrino.

Comparing the weak interaction rate, $\Gamma \sim T^5/M_W^4$, to the expansion rate, $H \sim T^2/M_{\rm Pl}$, one finds that neutrino are in thermal equilibrium at temperatures $T \gg 1$ MeV and decouple from the rest of plasma at lower temperatures. (One can do this in full detail, see e.g. [60].) Therefore, standard model neutrinos, which have small masses, decouple when they are still relativistic. The number density of neutrino at this time is given by Eq. (14). Below this temperature, neutrinos are no longer in thermal equilibrium with the rest of the plasma, and their temperature simply decreases as $T \propto 1/a$. However, the cosmological background of photons is heated up by the e^+e^- annihilations. Let us find a relation between T_ν and T_γ, which will also give the relation between n_ν and n_γ.

The annihilation reaction rate is much faster than the expansion of the universe, therefore this process is adiabatic, and entropy in comoving volume is conserved, $g_*\, T^3 = \mathrm{const}$, see Eq.(11). Before annihilation $g_* = g_\gamma + g_e \cdot (7/8) = 2 + 4 \cdot (7/8) = 11/2$. After annihilation $g_* = g_\gamma = 2$. Since before annihilation $T_\nu = T_\gamma$, we find $T_\nu = (4/11)^{1/3}\, T_\gamma$, and for one neutrino flavour we have

$$n_\nu = \frac{3}{11}\, n_\gamma \ . \tag{77}$$

Here we used Eq. (14) and $g_\gamma = g_\nu = 2$, since right handed neutrino do not contribute (are not excited) even if neutrino has a small Dirac mass, see Ref. [60]. As a consequence of e^+e^- annihilation neutrino temperature is lower. With $T_\gamma = 2.728$ K we find $T_\nu = 1.947$ K and $n_\nu = 115\ \mathrm{cm}^{-3}$.

At temperatures larger than neutrino mass, $T_\nu \gg m_\nu$, in the standard model, assuming no chemical potential, we find

$$\Omega_\nu = 3\, \left(\frac{7}{8}\right) \left(\frac{4}{11}\right)^{4/3}\, \Omega_\gamma \approx 0.68\, \Omega_\gamma \ , \tag{78}$$

where the factor of 3 corresponds to the number of neutrino flavours. This result allows us to find the epoch of equal matter and radiation densities

$$1 + z_{\rm eq} = \frac{\Omega_M}{\Omega_\gamma + \Omega_\nu} \approx 3200 \ . \tag{79}$$

Assume that by now neutrino became non-relativistic, i.e. their masses are larger than the present temperature. In this case, neutrino energy density is given by $\rho_\nu = \sum_i m_{\nu i}\, n_{\nu i}$. Since it has to be smaller than $\Omega_m\, \rho_c$, we have the constraint [75]

$$\sum_i m_{\nu i} < 94\ \Omega_m h^2\ \mathrm{eV} = 12\ \mathrm{eV} \ . \tag{80}$$

For dark matter particles to boost the structure formation, their typical velocities squared at the time of recombination should be smaller than the depth of typical gravitational wells, $v^2 \ll 10^{-5}$. In other words, the dark matter should be *cold*. This is not the case for particles as light as those which satisfy the bound Eq. (80). Neutrino can make up dark matter, but it will be *hot* dark matter.

Neutrino mass is pinned down. Free streaming of relativistic neutrinos suppresses the growth of fluctuations until ν becomes nonrelativistic at $z \sim m_j/3T_0 \sim 1000\ (m_j/\mathrm{eV})$. This effect of free-streaming is not seen in the data and therefore only small corrections due to light neutrino are allowed in the standard CDM picture. Combined CMBR and LSS analysis yields the constraint [9]

$$\Omega_\nu h^2 \ = \ \frac{\sum_i m_i}{93.5\ \mathrm{eV}} \ < \ 0.0076\ , \tag{81}$$

which translates into the upper bound

$$\sum_i m_i \ < \ 0.7\ \mathrm{eV} \qquad (95\%\ \mathrm{CL})\ . \tag{82}$$

On the other hand, atmospheric neutrino oscillations provide a lower bound on the heaviest neutrino mass, since $\sqrt{\delta m^2_{\mathrm{atm}}} \sim 0.03$ eV. Combining these two limits

$$0.03\ \mathrm{eV} \ \leq \ m_{\mathrm{heaviest}} \ \leq \ 0.24\ \mathrm{eV} \tag{83}$$

we see that the heaviest neutrino mass is now known to within an order of magnitude [76].

Can neutrino make up a galaxy halo? By $z \sim 1$ the neutrino quanta satisfying the mass bound Eq. (83) became sufficiently non-relativistic to make their way into gravitational wells. The question arises, can neutrino at least make up the dark halos and be responsible for flat rotational curves? The answer to this question is: no. To prove it, let us assume that neutrino does build up a dark matter halo with a flat rotational curve

$$\rho_{\mathrm{DM}} = \frac{M_{Pl}^2 v_{\mathrm{rot}}^2}{r^2}\ . \tag{84}$$

We can express the energy density $\rho_{\mathrm{DM}} = \rho_\nu$ through the integral of phase space density over the momenta

$$\rho_\nu = \frac{m_\nu}{(2\pi)^3}\int d^3k\ n(k,r)\ , \tag{85}$$

But for fermions, the phase-space density, $n(k,r) = n(E)$, should obey the Pauli exclusion principle, $n(E) < 1$. Combining Eqs. (84) and (85), we find $m^4 v^3 \sim M_{Pl}^2 v^2/r^2$, or

$$m_\nu > 120\ \mathrm{eV}\left(\frac{100\ \mathrm{km\ s^{-1}}}{v_{\mathrm{rot}}}\right)^{1/4}\left(\frac{1\ \mathrm{kpc}}{r_c}\right)^{1/2} \tag{86}$$

For dwarf galaxies this constraint (the Tremaine-Gunn limit [77]) reads $m_\nu > 500$ eV, and we arrive to contradiction with Eq. (80), which becomes even stronger when compared with Eq. (83).

Cosmological density of other thermal relics. Assume now some weakly interacting particle has a mass larger 1 MeV and decouples when it is non-relativistic. The equilibrium number density will be Boltzmann-suppressed in this case, by the exponent $\exp(-m/T)$. The weak interaction cross-section implies $\sigma \sim m^2/M_W^4$, if $m \ll M_W$. Repeating calculations for abundances, one finds that in this case $\Omega_m h^2 \approx 3\ (1\ \mathrm{GeV}/m)^2$, i.e. a correct cosmological abundance of dark matter would be achieved for $m \approx 5$ GeV.

On the other hand, if $m \gg M_W$, the annihilation crosssection becomes $\sigma \sim 1/m^2$ and one finds $\Omega_m h^2 \approx (m/1\ \mathrm{TeV})^2$, i.e. the correct cosmological abundance of dark matter is achieved for $m \approx 300$ GeV. Using field-theoretical unitarity and the observed density of the Universe, it can be shown that a stable elementary particle which was once in thermal equilibrium cannot have a mass greater than 340 TeV [78].

Cosmological density of non-thermal relics. The mass of non-thermal relics can be much larger than $O(10^2)$ TeV without violating unitarity bound; it can also be much smaller than than $O(1)$ GeV and dark matter still will be cold, as required by observations.

1. Axions. Very light scalar particles, like axions, are created in a state of coherent oscillations. This can be viewed also as a Bose-condensate. To illustrate the general idea, let us consider a scalar field with potential $V(\phi) = m^2\phi^2/2$. The equations of motion for the Fourier modes with a momentum k in an expanding Universe are

$$\ddot{\phi}_k + 3H\dot{\phi}_k + (k^2 + m^2)\phi_k = 0 \; . \tag{87}$$

Since the term $\propto H$ can be understood as friction, amplitude of those modes for which $9H^2 \gg (k^2+m^2)$ (almost) does not change with time. The oscillations of modes with a given k commence when H becomes sufficiently small, $9H^2 \ll (k^2 + m^2)$. Oscillating modes behave like particles, and their amplitude decreases with expansion. Since modes with the largest k start oscillations first, they will have the smallest amplitude and the field becomes homogeneous on a current horizon scale. Modes with all k will be already oscillating when $3H \approx m$, and will behave like cold dark matter since then. Note that the field will be homogeneous on the horizon scale at this time, but may be inhomogeneous on larger scales. This may lead to formation of dense clumps, "axion mini-clusters" [79, 80] of the mass $M \sim 10^{-12}\, M_\odot$ [81]. Note also that in the case of axions, one has to take into account the dependence of m on temperature T. Solving $3H(T) = m(T)$ one finds $\Omega_{\rm axion} \sim 1$ when $f_a \sim 10^{12}$GeV [82, 83].

2. Superheavy dark matter. Non-conformal quantum fields cannot be kept in a vacuum in an expanding universe. This can be understood on the example of a scalar field, Eq. (87). In conformal time, Eq. (24), and for rescaled field, $u_k \equiv \phi_k\, a$, the mode equations take form of an oscillator equation

$$\ddot{u}_k + \omega_k^2 u_k = 0 \; , \tag{88}$$

with time-dependent frequency

$$\omega_k^2 = k^2 + a^2 m^2 - \frac{\ddot{a}}{a}(1 - 6\xi) \; . \tag{89}$$

The constant ξ describes the coupling to the scalar curvature, corresponding term in the Lagrangian is $\xi R\phi$. The case of $\xi = 0$ corresponds to minimal coupling (Eq. (87) was written for this case), while $\xi = 1/6$ is the case of conformal coupling. Equations for massless, conformally coupled quanta are reduced to the equation of motion in Minkowski space-time. Particle creation does not occur in this case. For massive particles, conformal invariance is broken and particles are created regardless of the value of ξ. Let us consider the case of $\xi = 1/6$ (the general situation is considered in [84]). It is the particle mass which couples the system to the background expansion and serves as the source of particle creation in this case. Therefore, we expect that the number of created particles in comoving volume is $\propto m^3$ and the effect is strongest for the heaviest particles. In fact, stable particles with $m > 10^9$ GeV would overclose the Universe in the standard "pre-inflationary" Friedmann model [71]. Inflation cuts the particle production and $\Omega_{\rm SH} \sim 1$ if $m > 10^{13}$ GeV and reheating temperature is $T \sim 10^9$ GeV, which is the value of reheating temperature compatible with supergravity models [70, 71, 84].

7. BASICS OF INFLATION

In frameworks of "classical" cosmology and assuming no fine-tuning, one concludes that a typical universe should have had Plankian size, live Plankian time and contain just a few particles. This conclusion is based on the observation that Fridmann equations contain a single dimension-full parameter $M_{\rm Pl} \sim 10^{19}$ GeV, while dimensionless parameters naturally are expected to be of order unity. Yet, the observable Universe contains 10^{90} particles in it and had survived 10^{65} Plankian times. Where does it all came from? In other words, why is the Universe so big, flat ($\Omega_0 \approx 1$) and old ($t > 10^{10}$ years), homogeneous and isotropic ($\delta T/T \sim 10^{-5}$), why does it contain so much entropy ($S > 10^{90}$) and does

not contain unwanted relics like magnetic monopoles? These puzzles of classical cosmology were solved with the invention of Inflation [85, 86, 87, 88, 89]. All these questions are related to the initial conditions and one can simply postulate them. The beauty of Inflation is that it prepares these unnatural initial conditions of Big Bang, while the pre-existing state (which can be arbitrary to a large extent) is forgotten. Inflationary theory came with unplanned bonuses. Not only does the Universe become clean and homogeneous during inflation, but also the tiny perturbations necessary for the genesis of galaxies are created with the correct magnitude and spectrum. Below we consider the basics of inflationary cosmology.

7.1 Big Bang puzzles and Inflationary solutions

Horizon problem and the solution. The size of a causally connected region (horizon) scales in proportion to time, $R_{\rm H} \propto t$. On the other hand, the physical size of a given patch grows in proportion to the scale factor, $R_{\rm P} \propto\ a(t) \propto t^{\gamma}$. The exponent γ depends upon the equation of state, $\gamma = 1/2$ for radiation and $\gamma = 2/3$ for matter dominated expansion. In any case, for the "classical" Friedmann Universe $\gamma < 1$ and the horizon expands faster than volume. Take the largest visible patch today. It follows that in the past its physical size should have been larger than the horizon size at the time (since they are equal today) and therefore this patch should have contained many casually disconnected regions. For example, as we have found in Section 3., the angular size of horizon at the moment of last scattering is $\approx 2^{\circ}$, see Eq. (55), which tells us that we observe 10^4 causally disconnected regions at the surface of last scattering. The question arises, why is the Universe so homogeneous at large scales?

This problem can be solved if during some period of time the volume had expanded faster than the horizon. During such a period, the whole visible Universe can be inflated from one ("small") causally connected region. Clearly, this happens if $\gamma > 1$, which means $\ddot{a} > 0$. Either of these two conditions can be used as definition of an inflationary regime. Using the Friedmann equation (6) we find that the inflationary stage is realized when $p < -\rho/3$. In particular, if $p = -\rho$ the energy density remains constant during expansion in accord with the first law of thermodynamics, Eq. (7), and the physical volume expands exponentially after a few Hubble expansion times, $a(t) = {\rm e}^{Ht}$, see Eq. (5).

Curvature problem and the solution. The Friedmann equation (5) can be re-written as

$$k = a^2 \left(\frac{8\pi G}{3}\, \rho - H^2 \right) = a^2 H^2\ (\Omega - 1) = \dot{a}^2\ (\Omega - 1) = {\rm const.} \tag{90}$$

Here we immediately see the problem: during matter or radiation dominated stages, $\dot{a}^2$ decreases (in general, this happens for any expansion stage with $\ddot{a} < 0$), therefore Ω is driven away from unity. To observe $\Omega\ \sim\ 1$ today, the observer has to live in a universe with extreme initial fine-tuning, say at the epoch of nucleosynthesis, when temperature was $T \sim 1$ MeV, one finds $|\Omega(t_{\rm NS}) - 1| < 10^{-15}$, and even stronger tuning is required at earlier epochs. A possible solution is obvious: accelerated expansion $\ddot{a} > 0$ increases $\dot{a}$ and therefore drives $\Omega(t)$ to unity. A robust, crucial and testable prediction of inflationary cosmology is a flat Universe, $\Omega = 1$.

The problem of Entropy. As we know already, the energy of a vacuum, $p = -\rho$, stays constant despite the expansion. In this way, room for matter full of energy could have been created. The vacuum energy is converted into particles and radiation at some later stage and, in particular, the observed huge entropy is created. Potentially, this mechanism works for any inflationary scenario, since the product ρa^3 is guaranteed to grow whenever $\ddot{a} > 0$. However, the important question is whether a graceful exit out of the inflationary stage and successful reheating is possible. In practice, this issue has killed a number of inflationary models. Remarkably, the original model by A. Guth [86] had being ruled out precisely on these grounds [90].

Inflation has to continue for a sufficiently long time for the problems of horizon, curvature and entropy to be solved. All these give roughly the same condition on the number of required "e-foldings"

of inflation [86] and we consider here a (simplified) derivation based on entropy. A precise condition can be found e.g. in Ref. [91]. Multiplying the current temperature in the universe by its visible size we find $Ta\chi_0 \sim 10^{30}$, where χ_0 is the comoving size of the present horizon. The product Ta conserves (up to the change in the number of relativistic degrees of freedom, which we neglect here) since the Universe expansion is adiabatic after the end of Inflation, see Eq. (11). Let T_r denote the reheating temperature and $\mathrm{e}^N \equiv a_f/a_i$ the number of inflationary "e-foldings", where a_f is the value of scale factor at the end of inflation and a_i at its beginning, respectively. We also want at least the whole visible universe to be inflated out of a single causally connected patch, which gives $a_i\chi_0 \sim H_i^{-1}$, where H_i is the value of the Hubble parameter during Inflation. All this gives the condition[1]

$$\frac{T_r}{H_i}\ \mathrm{e}^N \gtrsim 10^{30}\ . \tag{91}$$

In popular models of Inflation the ratio T_r/H_i is within a couple orders of magnitude from unity, and we find $N \gtrsim 65$.

7.2 Models of Inflation

Consider $T_{\mu\nu}$ for a scalar field φ

$$T_{\mu\nu} = \partial_\mu\varphi\,\partial_\nu\varphi - g_{\mu\nu}\,\mathcal{L} \tag{92}$$

with the Lagrangian :

$$\mathcal{L} = \partial_\mu\varphi\,\partial^\mu\varphi - V(\varphi)\ . \tag{93}$$

In a state when all derivatives of φ are zero, the stress-energy tensor of a scalar field simplifies to $T_\mu^\nu = V(\varphi)\,\delta_\mu^\nu$. This corresponds to a vacuum state. Indeed, comparing with Eq. (4), we find $V = \rho = -p$. There are two basic ways to arrange $\varphi \approx$ const and hence to imitate the vacuum-like state.

1. Consider the potential $V(\phi)$, which has a local minimum with a non-zero energy density separated from the true ground state by a potential barrier [86]. A universe which happened to be trapped in the meta-stable minimum will stay there for a while (since such a state can decay only via subbarrier tunneling) and expansion of the universe will diminish all field gradients. Then the Universe enters a vacuum state. This model is ruled out since the inhomogeneities created during the phase transition which terminates the inflationary phase are too large [90]. However, the model is good for illustration purposes. The frequently asked question is: how can it be that the energy density stays constant despite the expansion? In the model with local potential minimum the energy cannot decrease (classically) below the local minimum value, and therefore it has to stay constant despite the expansion.

2. A. Linde was first to realize that things work in the simplest possible setup [89]. Consider the potential

$$V(\phi) = \frac{1}{2}m_\phi^2\phi^2\ . \tag{94}$$

The equation of field motion in an expanding Universe is $\ddot{\phi}+3H\dot{\phi}+m_\phi^2\phi = 0$. If $H \gg m$, the "friction" is too big and the field (almost) does not move. Therefore time derivatives in $T_{\mu\nu}$ can be neglected, and inflation starts (in a sufficiently homogeneous patch of the Universe). A Hubble parameter in this case is determined by the potential energy, $H \approx m\phi/M_{\rm Pl}$, and we see that inflation starts if the initial field value happens to satisfy $\phi > M_{\rm Pl}$. During inflationary stage the field slowly rolls down the potential hill. This motion is very important in the theory of structure creation; inflation ends when $\phi \sim M_{\rm Pl}$. At this time, field oscillations start around the potential minimum and later decay into radiation. In this way matter was likely created in our Universe.

[1] Strictly speaking in this relation T_r is not the real temperature in a state of thermal equilibrium, but $T_r \sim \rho_r^{1/4}$, where ρ_r is the energy density at the moment when the expansion becomes dominated by relativistic particles.

7.3 Unified theory of Creation

During Inflation and by its end the Universe was in a vacuum-like state. We have to figure out how this "vacuum" was turned into the matter we observe around us, and how primordial fluctuations which gave rise to galaxies were created. Fortunately, these problems can be formalized in a nice and unified way. Basically, everything reduces to a problem of particle creation in a time-dependent classical background. On top of every "vacuum" there are fluctuations of all quantum fields which are present in a given model. This bath of virtual quanta is indestructible, and even Inflation cannot get rid of it. Being small, fluctuations of any field obey an oscillator equation

$$\ddot{u}_k \; + \; [k^2 + m^2_{\rm eff}(\eta)] \; u_k = 0 \, , \tag{95}$$

here u_k are amplitudes of fluctuating fields in Fourier space. Effective mass becomes time dependent through the coupling to time-dependent background. Because $m_{\rm eff}$ is time dependent, it is not possible to keep fluctuations in a vacuum. If one arranges to put oscillators with momentum k into the vacuum at one time, they will not be in vacuum at a latter time because positive and negative frequency solutions mix, see below. Several remarks are in order.

- Eq. (95) is valid for all particle species.
- The equation looks that simple in a conformal reference frame $ds^2 = a(\eta)^2 \; (d\eta^2 - dx^2)$. (Everywhere in this chapter a "dot" means derivative with respect to η.)
- Of particular interest are ripples of space-time itself: curvature fluctuations (scalar fluctuations of the metric) and gravity waves (tensor fluctuations of the metric).
- Effective mass $m_{\rm eff}$ can be non-zero even for massless fields. Gravitational waves give the simplest example [92], with $m^2_{\rm eff} = -\ddot{a}/a$. The effective mass for curvature fluctuations has a similar structure $m^2_{\rm eff} = -\ddot{z}/z$, but with a being replaced by $z \equiv a\dot{\phi}/H$, see Refs. [93, 94, 95, 96].
- For conformally coupled, but massive scalar $m_{\rm eff} = m_0 \, a(\eta)$.

Note that creation was only possible because nature is not conformally-invariant. Otherwise, $m_{\rm eff}$ is time-independent and vacuum remains vacuum forever. There are two important instances of time varying classical background in cosmology:

- Expansion of space-time, $a(\eta)$.
- Motion of the inflaton field, $\phi(\eta)$.

Both can be operational at any epoch of creation:

- During inflation (superhorizon size perturbations).
- While the inflaton oscillates (reheating).

During inflation superhorizon size perturbations of metric are created, which give seeds for Large Scale Structure (LSS) formation and eventually lead to the formation of galaxies, and therefore of the Solar system and all the rest which we can see around us. During reheating matter itself is created. Overall, there are four different situations (two sources times two epochs). If coupling to the inflaton is not essential, the corresponding process will be called "pure gravitational creation" in what follows.

There are several primary observables which can be calculated out of u_k and further used for calculation of quantities of interest. Most useful are:

- The particle occupation numbers, n_k. Integration over d^3k gives the particle number density.
- The power spectrum of field fluctuations, $P_k \equiv u^*_k u_k$. Integration over d^3k gives the field variance.

Depending on physical situation, only one or the other may have sense. The particle number in a comoving volume is useful because it

- is adiabatic invariant on sub-horizon scales (or when $m > H$);
- allows to calculate abundances of various relics, e.g. dark matter.

But it has no meaning at super-horizon scales when $m < H$. The power spectrum and/or field variance is useful because it

- does not evolve on super-horizon scales if $m < H$;
- allows to calculate density perturbations generated during inflation;
- is crucial for dynamics of phase transitions;
- helps to calculate back-reaction in a simple way (Hartree approximation).

But P_k evolves on sub-horizon scales and when $m > H$.

Let me start with the discussion of metric perturbations.

Gravitational creation of metric perturbations. As an important and simple example, let us consider quantum fluctuations of a real scalar field, which we denote as φ. It is appropriate to rescale the field values by the scale factor, $\varphi \equiv \phi/a(\eta)$. This brings the equations of motion for the field ϕ into a simple form of Eq. (95). As usual, we decompose ϕ over creation and annihilation operators $b_{\mathbf{k}}$ and $b^\dagger_{\mathbf{k}}$

$$\phi(\mathbf{x},\eta) = \int \frac{d^3k}{(2\pi)^{3/2}} \left[u_k(\eta)\, b_{\mathbf{k}}\, \mathrm{e}^{i\mathbf{kx}} + u^*_k(\eta)\, b^\dagger_{\mathbf{k}}\, \mathrm{e}^{-i\mathbf{kx}}\right] . \tag{96}$$

Mode functions u_k satisfy Eq. (95). In what follows we will assume that φ is the inflaton field of the "chaotic" inflationary model, Eq. (94). During inflation $H \gg m$ and $H \approx \mathrm{const}$. So, to start with, we can assume that φ is a massless field on the constant deSitter background. (The massive case can be treated similarly, but analytical expressions are somewhat more complicated and do not change the result in a significant way. Corrections due to change of H can also be taken into account, and we do that later for the purpose of comparison with observations.) With a constant Hubble parameter during inflation the solution of Friedmann equations in conformal time is

$$a(\eta) = -\frac{1}{H\eta} \tag{97}$$

and the equation for mode functions of a massless, conformally coupled to gravity ($\xi = 0$), scalar field takes the form

$$\ddot{u}_k + k^2 u_k - \frac{2}{\eta^2}\, u_k = 0 . \tag{98}$$

Solutions which start as vacuum fluctuations in the past ($\eta \to -\infty$) are given by

$$u_k = \frac{\mathrm{e}^{\pm ik\eta}}{\sqrt{2k}} \left(1 \pm \frac{i}{k\eta}\right) . \tag{99}$$

Indeed, at $\eta \to -\infty$ the second term in the parentheses can be neglected and we have the familiar mode functions of the Minkowski space time. The wavelength of a given mode becomes equal to the horizon size (or "crosses" the horizon) when $k\eta = 1$. Inflation proceeds with $\eta \to 0$, so the modes with progressively larger k cross the horizon. After horizon crossing, when $k\eta \ll 1$, the asymptotics of mode functions are

$$u_k = \pm\frac{i}{\sqrt{2}k^{3/2}\eta}, \quad \text{or} \quad \varphi_k = \frac{u_k}{a(\eta)} = \mp\frac{iH}{\sqrt{2}k^{3/2}} . \tag{100}$$

The field variance is given by

$$\langle 0|\phi^2(x)|0\rangle = \int \frac{d^3k}{(2\pi)^3}\, |\varphi_k|^2 . \tag{101}$$

and we find in the asymptotic (the careful reader will recognize that this is already regularized expression with zero-point fluctuations being subtracted)

$$\langle\varphi^2\rangle = \frac{H^2}{(2\pi)^2} \int \frac{dk}{k} . \tag{102}$$

Defining the power spectrum of the field fluctuations as a power per decade, $\langle\varphi^2\rangle \equiv \int P_\varphi(k)\, d\ln k$, we find

$$P_\varphi(k) = \frac{H^2}{(2\pi)^2} . \tag{103}$$

Curvature perturbations. According to Eq. (3), the three-dimensional curvature of space sections of constant time is inversely proportional to the scale factor squared, ${}^{(3)}R \propto a^{-2}$. Therefore, the perturbation of spatial curvature is proportional to $\delta a/a$, and this ratio can be evaluated as

$$\zeta \equiv \frac{\delta a}{a} = H\delta t = H\,\frac{\delta\varphi}{\dot\varphi}\ . \tag{104}$$

This allows to relate the power spectrum of curvature perturbations to the power spectrum of field fluctuations

$$P_\zeta(k) = \frac{H^2}{\dot\varphi^2}\ P_\varphi(k)\ , \tag{105}$$

and we find for the power spectrum of curvature perturbations

$$P_\zeta(k) = \frac{1}{4\pi^2}\ \frac{H^4}{\dot\varphi^2}\ . \tag{106}$$

This very important relation describes inflationary creation of primordial perturbations, and can be confronted with observations. The usefulness of curvature perturbations for this procedure can be appreciated in the following way:

1. Consider the perturbed metric, Eq. (46). The product $a(1-\Phi)$ for the long-wavelength perturbations can be viewed as a perturbed scale factor, i.e. $\delta a/a = -\Phi$. Comparing this relation with Eq. (104) and Eq. (50), we find for the temperature fluctuations which are of the superhorizon size at the surface of last scattering

$$\frac{\delta T}{T} = \frac{2}{3}\ \zeta_k\ . \tag{107}$$

2. On superhorizon scales the curvature perturbations do not evolve.[2] This fact allows to relate directly the observed power spectrum of temperature fluctuations to the power spectrum of curvature fluctuations generated during inflation.

Tensor perturbations. Mode functions of gravity waves (after rescaling by $M_{\rm Pl}/\sqrt{32\pi}$) obey the same equation as mode functions of massless minimally coupled scalar [92]. Using the result Eq. (103) we immediately find [97]

$$P_T(k) = 2\ \frac{32\pi}{M_{\rm Pl}^2}\ P_\varphi(k) = \frac{16}{\pi}\ \frac{H^2}{M_{\rm Pl}^2}\ , \tag{108}$$

where the factor of 2 accounts for two graviton polarizations.

Slow-roll approximation. During inflation, the field φ rolls down the potential hill very slowly. A reasonable approximation to the dynamics is obtained by neglecting $\ddot\varphi$ in the field equation $\ddot\varphi + 3H\dot\varphi + V' = 0$. This procedure is called the slow-roll approximation

$$\dot\varphi \approx -\frac{V'}{3H}\ . \tag{109}$$

Field derivatives can also be neglected in the energy density of the inflaton field, $\rho \approx V$

$$H^2 = \frac{8\pi}{3M_{\rm Pl}^2}\,V\ . \tag{110}$$

This gives for curvature perturbations

$$\zeta_k \equiv P_\zeta(k)^{1/2} = \frac{H^2}{2\pi\ \dot\varphi} = \frac{4H}{M_{\rm Pl}^2}\ \frac{V}{V'}\ . \tag{111}$$

[2] I should warn that this is quite a generic statement and does holds in situations usually considered. Thus, it is forgotten sometimes that this is not a universally true statement. To avoid possible confusion when encountering specific complicated models, the reader should keep this fact in mind.

Normalizing to CMBR. As an example, let us consider the simplest model $V = \frac{1}{2}m^2\varphi^2$. We have

$$\frac{V}{V'} = \frac{\varphi}{2}, \qquad \text{and} \quad H = \sqrt{\frac{4\pi}{3}}\frac{m\varphi}{M_{\rm Pl}} \, . \tag{112}$$

This gives for the curvature fluctuations

$$\zeta_k = \sqrt{\frac{16\pi}{3}} \, \frac{m\,\varphi^2}{M_{\rm Pl}^3} \, . \tag{113}$$

Using the relation between curvature and temperature fluctuations, Eq. (107), and normalizing $\delta T/T$ to the measured value at largest l, which is $\delta T/T \sim 10^{-5}$ (see Fig. 5) we find the restriction on the value of the inflaton mass in this model:

$$m \approx \frac{\delta T}{T} \, \frac{M_{\rm Pl}}{30} \approx 10^{13} \ \ {\rm GeV} \, . \tag{114}$$

Here I have used the fact that in this model the observable scales cross the horizon when $\varphi \approx M_{\rm Pl}$.

Slow-roll parameters. The number of e-foldings ($a = {\rm e}^{Ht} \equiv {\rm e}^N$) of inflationary expansion from the time when $\varphi = \varphi_i$ to the end can be found as

$$N(\varphi_i) = \int_{t_i}^{t_f} H(t)dt = \int \frac{H}{\dot\varphi} \, d\varphi = \frac{8\pi}{M_{\rm Pl}^2} \int_{\varphi_e}^{\varphi_i} \frac{V}{V'} \, d\varphi \, . \tag{115}$$

In particular, in the model Eq. (94) we find that the largest observable scale had crossed the horizon ($N \sim 65$) when $\varphi_i \approx 3.5 M_{\rm Pl}$. All cosmological scales which fit within the observable universe encompass a small $\Delta\phi$ interval within $M_{\rm Pl} < \varphi < \varphi_i$. And inflaton potential should be sufficiently flat over this range of $\Delta\phi$ for the inflation to proceed. This means that observables essentially depend on the first few derivatives of V (in addition the the potential $V(\phi_0)$ itself). From the first two derivatives one can construct the following dimensionless combinations

$$\epsilon \equiv \frac{M_{\rm Pl}^2}{16\pi} \left(\frac{V'}{V}\right)^2 \, , \tag{116}$$

$$\eta \equiv \frac{M_{\rm Pl}^2}{8\pi} \frac{V''}{V} \, , \tag{117}$$

which are often called the slow-roll parameters.

The power spectra of curvature, Eq. (105), and of tensor perturbations, Eq. (108), in slow-roll parameters can be rewritten as

$$P_\zeta(k) = \frac{1}{\pi\epsilon}\frac{H^2}{M_{\rm Pl}^2}, \qquad P_T(k) = \frac{16}{\pi}\frac{H^2}{M_{\rm Pl}^2} \, . \tag{118}$$

Comparing these two expressions we find

$$\frac{P_T(k)}{P_\zeta(k)} = 16\epsilon \, . \tag{119}$$

Primordial spectrum. In general, the spectra can be approximated as power law functions in k:

$$P_\zeta(k) = P_\zeta(k_0) \left(\frac{k}{k_0}\right)^{n_S - 1} \, , \tag{120}$$

$$P_T(k) = P_T(k_0) \left(\frac{k}{k_0}\right)^{n_T} \, . \tag{121}$$

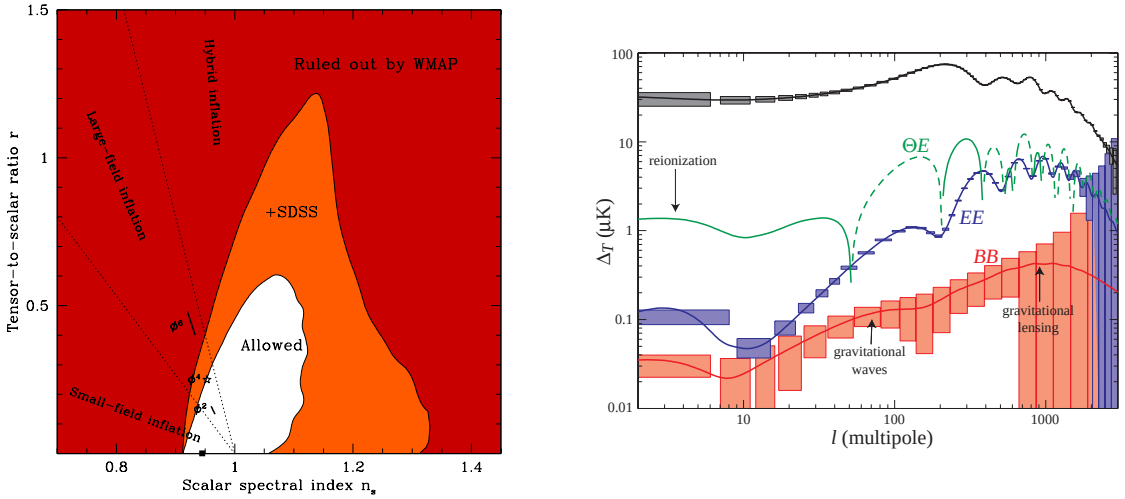

Fig. 20: **Left panel:** 95% constraints on inflationary models in the (n_s, r) plane. From Ref. [10]. **Right panel:** Forecast for the planned ESA Planck mission.

To the first approximation, H in Eq. (118) is constant. Therefore, in this approximation, power spectra do not depend on k and $n_S = 1$, $n_T = 0$. This case is called the Harrison-Zel'dovich spectrum [98, 99] of primordial perturbations. However, in reality, H is changing, and in Eq (118) for every k one should take the value of H at the moment when the relevant mode crosses horizon. In slow roll parameters one then finds (see e.g. Ref. [100] for the nice overview)

$$n_S = 1 + 2\eta - 6\epsilon, \qquad n_T = -2\epsilon \; . \tag{122}$$

We can re-write Eq. (123) as a relation between the slope of tensor perturbations and the ratio of power in tensor to curvature modes

$$\frac{P_T(k)}{P_\zeta(k)} = -8 n_T \; . \tag{123}$$

This is called the *consistency relation* to which (simple) inflationary models should obey.

Different models of inflation have different values of slow-roll parameters η and ϵ, and therefore can be represented in the (η,ϵ) parameter plane. Using the relations Eq. (122) we see that this plane can be mapped into (n_S, n_T), or using also Eq. (123) into the (n_S, r) parameter plane, where r is the ratio of power in tensor to scalar (curvature) perturbations. In this way, different inflationary models can be linked to observations and constraints can be obtained.

The most recent constraints in the (n_s, r) plane, utilizing WMAP and SDSS data, are presented in Fig. 20, the left panel. The shaded dark red region is ruled out by WMAP alone. The shaded light red region is ruled out when adding SDSS information. The two dotted lines delimit the three classes of inflationary models known as the small-field, large-field and hybrid models. Some single-field models of inflation make highly specific predictions in this plane, as indicated. From top to bottom, the figure shows the predictions for $V(\phi) \propto \phi^6$ (line segment; ruled out by CMB alone), $V(\phi) \propto \phi^4$ (star; on verge of exclusion) and $V(\phi) \propto \phi^2$ (line segment; the inflation model Eq. (94); still allowed).

Testing inflation. All predictions of Inflationary cosmology, which could have being tested so far, have being confirmed. In particular, the Universe is spatially flat (within experimental errors), $\Omega = 1.02 \pm 0.02$, see Table I. The primordial perturbations are of superhorizon size and adiabatic. The spectral index is close to the Harrison-Zeldovich case, see Fig. 20, the left panel. Crucial test of inflationary

models would be detection of gravity waves and verification of the consistency relation. This signatures of typical inflationary models are within reach of future CMBR experiments, see Fig. 20, the right panel.

8. Ultra-High Energy Cosmic Rays

In early years, cosmic ray studies were ahead of accelerator research, starting from the discovery of positrons, through muons, to that of pions and strange particles. Today we are facing the situation that the puzzling saga of cosmic rays of the highest energies may again unfold in the discovery of new physics, now beyond the Standard Model; or it may bring to life an "extreme" astrophysics.

Immediately after the discovery of the relict Cosmic Microwave Background Radiation (CMBR), Greisen, Zatsepin and Kuzmin [101, 102] have realized that the highest energy protons should catastrophically loose energy in photo-production of pions on this universal background. This process limits the distance to the farthest sources of observed rays to be roughly 100 Mpc and should lead to the cut-off in the energy spectrum. However, the number of events with energies beyond the expected cut-off as measured by different installations is growing with time [103, 104, 105, 106, 107, 108, 109], while no nearby sources where identified. The findings of Greisen, Zatsepin and Kuzmin (GZK) are based on solid fundamental physics which involve precisely measured cross-sections in a GeV energy range (in the center of mass reference frame). Therefore, if the data are correct – and it is believed they are basically correct[3] – one should either invoke new physics, or accept unconventional and uncomfortable very "extreme" astrophysics. This is the reason for the excitement and growing interest in ultra-high energy cosmic ray research; for recent reviews see [110, 111, 112, 113].

Methods of detection. At energies below 10^{14} eV, the flux of cosmic rays is sufficiently high that direct measurements using high altitude balloons or satellite experiments are possible. Above 10^{15} eV, the flux is only one particle per m^2 per year, which excludes direct observations on the orbit. At 10^{20} eV the number is down to one particle per square kilometer per century. Here the problem for direct measurements would be not only a vanishingly small flux, but the enormously high energy itself. (Remember that calorimeters at modern colliders weigh hundreds of thousands of tonnes.) Fortunately, the major part of our UHECR detectors is already built for us by Nature and is put, rotating, into orbit: the Earth's atmosphere makes a perfect calorimeter. The atmosphere is just thick enough so that showers of secondary particles produced by incoming cosmic rays of the highest energies, in collisions with nuclei of air, reach their maximum intensity just above the Earth's surface. Particles in a shower propagate with the velocity of light, forming a thin disk perpendicular to the direction of the incident particle. At 10^{19} eV the footprint of the shower on the ground is several kilometers across.

The shower can be registered either by placing an array of particle detectors on the earth's surface, or by measuring the Cherenkov light produced by particles in the atmosphere, or by tracking the fluorescence light emitted when shower particles excite nitrogen molecules of the air. Particle detectors in a ground array can be spaced hundreds of meters apart and are operational around the clock. Fluorescence light telescopes see the cosmic ray track just like a fly's eye would see the meteorite, but only moving with the speed of light. These detectors are operational only on clear moonless nights, but are able to measure the longitudinal shower profile and its maximum depth directly.

With either technique, the energy and incident direction of primary particle can be measured shower by shower. Chemical composition also can be inferred, but only in a statistical sense, after averaging over many showers.

1. *Arrival direction.* The timing of a signal in different detectors is used to determine the direction of a shower (ground array technique). Direction is measured with an accuracy of about 2°. The measurement is straightforward and does not involve any uncertainties. Inferred information is reliable.

[3] While recently a disagreement in measured fluxes has emerged, there is no reason for doubt in the reality of super-GZK events.

Fluorescence light telescopes observe the whole shower track, and in stereo mode the precision of angle determination is 0.5°.

2. *Energy.* Energy estimate, on the other hand, is not that straightforward. In fluorescent light detectors, the energy of primary particle is derived from the observed light intensity, therefore incorrect modeling and/or insufficiently frequent monitoring of atmosphere transparency can be a source of errors. For the ground array detectors, the energy estimate relies on a Monte-Carlo model of shower development and is related to the shower density profile. Nevertheless, the currently favored model, QGSJET [114], describes data well from TeV up to highest energies and it is believed that the overall error (statistical plus systematic) in energy determination does not exceed 30 %.

The best would be to employ both the ground array and fluorescent light techniques simultaneously. This should reduce systematic errors, and this is the design of the forthcoming Pierre Auger project [**?**].

3. *Chemical composition.* Chemical composition can be inferred from the details of shower development. For example, showers initiated by heavy nuclei start earlier in the atmosphere and have less fluctuations compared to proton showers. Fluorescence detectors observe shower development directly. Using ground array detectors, the shower depth can be extracted by measuring e.g. the ratio of electrons to muons. At lowest energies, the chemical composition of cosmic rays reflects primary and secondary element abundances; for a recent review see [115]; at highest energies, $E > 4 \times 10^{19}$ eV, the conclusion is that less than 50% of primary cosmic rays can be photonic at 95% confidence level [116].

8.1 Propagation of the ultra-high energy cosmic rays

In this subsection, we consider the influence of different cosmological backgrounds on the propagation of highest-energy cosmic rays.

Magnetic fields. Magnetic fields play an important role in the processes of cosmic ray acceleration and propagation, their trajectories being bent by the action of the Lorentz force

$$\frac{d\vec{v}}{dt} = \frac{Ze}{E} \ [\vec{v} \times \vec{B}] \ . \tag{124}$$

For a qualitative discussion, it is often sufficient to compare a gyro-radius of the trajectory of a relativistic particle

$$R_g = \frac{E}{ZeB} \tag{125}$$

to other relevant length scales of the problem. E.g., a magnetic "trap" can not confine a cosmic ray if the gyro-radius exceeds the trap size. The deflection angle $\Delta\theta$, after traversing the distance L in a homogeneous magnetic field, is proportional to $L/R_{\rm L}$. In a chaotic magnetic field, the deflection angle will grow as $\sqrt{L}$. Let us estimate a typical deflection angle, L/R_g, of a charged UHE particle after traversing Galactic or extra-galactic magnetic fields.

1. In the Galactic magnetic field, for particles coming across the Galactic disc, we have

$$\frac{\Delta\theta}{Z} \approx 2.5^\circ \ \frac{10^{20} \text{ eV}}{E} \ \frac{B}{3 \ \mu G} \ \frac{L}{1.5 \text{ kpc}} \ , \tag{126}$$

where $3\,\mu G$ is magnitude of the regular magnetic field and 1.5 kpc is the width of the disc. We see that protons with $E > 10^{18}$ eV escape our Galactic disk easily. Protons of smaller energy are trapped and can escape the Galaxy only by diffusion and "leaking" from the boundary. Cosmic rays with $E > 10^{18}$ eV should be extra-galactic, if protons. Even if CRs would be all iron nuclei, at $E > 2 \cdot 10^{19}$ eV cosmic rays

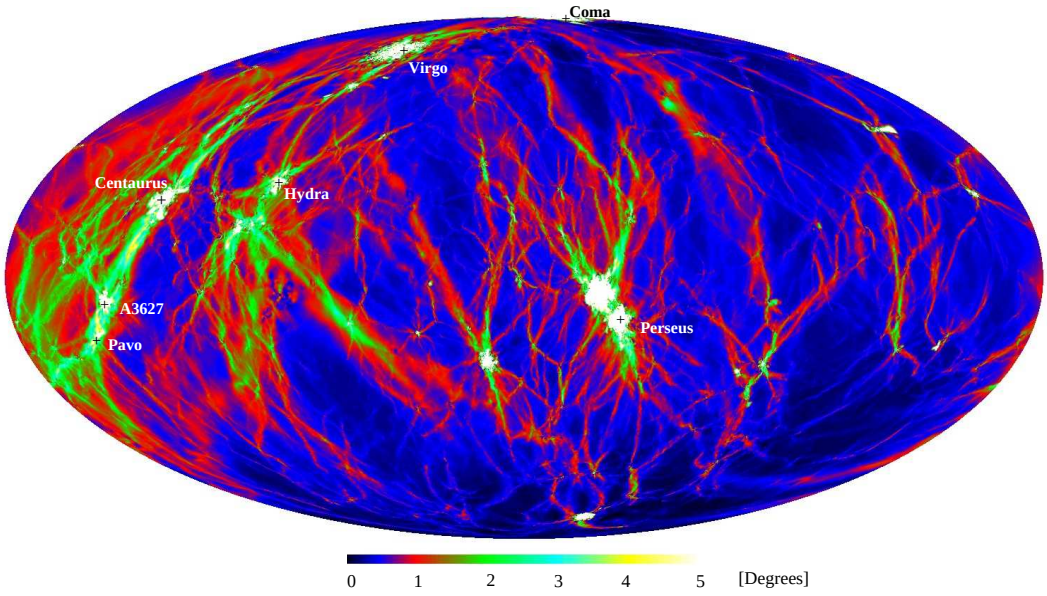

Fig. 21: Full sky map of deflection angles for UHECRs with energy 4×10^{19} eV after traveling 100 Mpc in an extra-galactic magnetic field. The coordinate system is galactic, with the galactic anti-center in the middle of the map. Positions of identified clusters are marked using the locations of the corresponding halos in the simulation. The map is obtained in a magneto-hydrodynamical simulation of cosmic structure formation that correctly reproduces the positions and masses of known galaxy clusters in the Local Universe. From Ref. [117]

should be extra-galactic, otherwise strong anisotropy in the direction of the Galactic disc would have been observed.

2. Extra-galactic magnetic fields have not yet been measured, except for the central regions of galaxy clusters [118]. However, there is an upper bound on their strength from the (absence of) Faraday rotation of polarized extra-galactic sources [119, 120]. This translates to the upper bound on deflections in extra-galactic magnetic fields

$$\frac{\Delta\theta}{Z} < 2.5^\circ \; \frac{10^{20}\ \mathrm{eV}}{E} \; \frac{B}{10^{-9}\ \mathrm{G}} \; \frac{(L\lambda)^{1/2}}{10\ \mathrm{Mpc}} \,, \tag{127}$$

where λ is the coherence length of an extra-galactic magnetic fields and is believed to satisfy $\lambda < 1$ Mpc. However, extragalactic fields are strongly inhomogeneous, with amplitude changing by orders of magnitude from clusters to filaments, and from filaments to voids. Deflections in some directions, which do not cross clusters and strong filaments, may be small, otherwise deflections can be very large. This situation cannot realistically be described by a mean field.

Only recently have attempts been made to simulate UHECR propagation in a realistically structured universe [117, 121]. Results of Ref. [117] are shown in Fig. 21. Additional motivation for this simulation was to obtain, in constraint simulations of the Local Structure, a realistic map of expected deflections, which would reflect the positions of known clusters. Such a map can be used in the analysis of cosmic ray arrival directions. Resulting deflections do not exceed the resolution of UHECR experiments over most of the sky. About an order of magnitude stronger deflections were obtained in Ref. [121]. There are two possible reasons for disagreement. First, simulations of Ref. [121] were unconstrained and therefore do not reflect our concrete local neighborhood. Second, variable resolution of Ref. [117] was better in cluster regions, which is a possible reason for the larger obtained dynamical range between fields in clusters and filaments. Since in both simulations the magnetic fields are normalized to typical values in the core of rich clusters, their values in the filaments will be very different, with larger fields

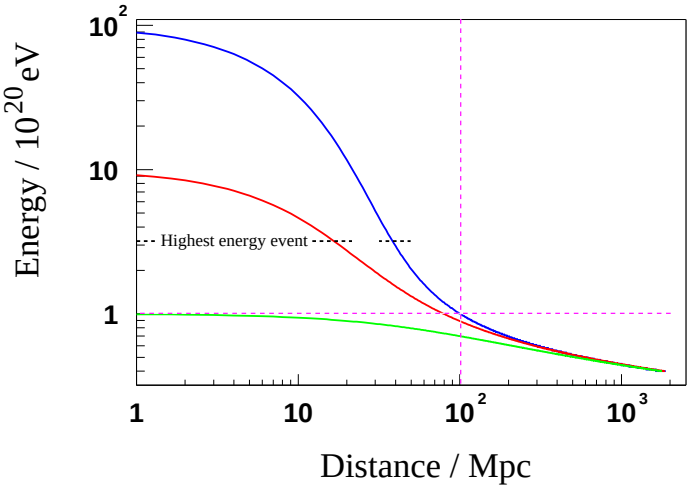

Fig. 22: Energy of protons as a function of the distance propagated in CMBR for three initial values of energy at the source, $10^{22},\ 10^{21}$ and 10^{20} eV respectively.

outside clusters in Ref. [121]. A work aimed to resolve these differences is in progress. For now, I adopt the results of Ref. [117] and conclude that arrival directions of UHECR should point back to the sources. Charged particle astronomy of UHECR is, in principle, possible.

Interactions with cosmic radiation backgrounds. Ultra-high energy cosmic rays cannot propagate elastically in cosmic backgrounds. They have enough energy to produce secondary particles even in collisions with CMBR (important for proton primaries) or radio photons (important for UHECR photons) or infrared radiation (important for propagation of nuclei). Most important is the reaction of pion photo-production for protons (or neutrons) propagating in relic cosmic microwave background left over from the Hot Big Bang. For the threshold energy of this reaction we find, in the laboratory frame,

$$E_{\rm th}(p+\gamma \to N+\pi) = \frac{(m_p+m_\pi)^2 - m_p^2}{2E_\gamma(1-\cos\theta)}\ . \tag{128}$$

Note, that in the derivation of this relation, standard Lorentz kinematic and standard dispersion relation between particle energy and momentum, $E^2 = k^2 + m^2$, are assumed. If any of these are violated, the threshold condition in a laboratory frame may look different. For the black body distribution of CMBR photons with temperature $T = 2.7^\circ\ K$ we find

$$E_{th} \approx 5 \times 10^{19}\ {\rm eV}\ . \tag{129}$$

This reaction has a large cross section, being the largest at the Δ resonance. At half-width of the resonance

$$\sigma \sim 300\ \mu b \approx 3 \times 10^{-28} {\rm cm}^2\ . \tag{130}$$

Density of CMB radiation is $n \sim T^3 \sim 400\ {\rm cm}^{-3}$. This corresponds to the mean free path:

$$L_\sigma = (\sigma n)^{-1} \approx 8 \times 10^{24}\ {\rm cm} \approx 2.7\ {\rm Mpc} \tag{131}$$

In each collision $\approx 20\%$ of energy is lost (which is the mass of a pion). Successive collisions rob protons of energy, which decreases exponentially. The distance over which energy decreases by one e-fold is

called the attenuation length. At the threshold, Eq. (129), the attenuation length is large, $L_A \approx 10^3$ Mpc (being determined by other processes, see below.) With increasing energy, it rapidly decreases and at energies above the Δ resonance for typical CMBR photons, $E \gtrsim 5 \cdot 10^{20}$ eV, the attenuation length is $L_A \approx 10$ Mpc. It follows that the energy of protons drops below 10^{20} eV after it travels the distance of order 100 Mpc almost independently upon initial energy, see Fig. (22). We conclude that

[**A1**] *Protons detected with* $E > 10^{20}$ eV *should have an origin within* $R < R_{\rm GZK} \equiv 100$ Mpc.

We will call the corresponding volume a GZK-sphere (or GZK-distance).

The reaction $p + \gamma \to p + e^+e^-$ is sub-dominant. While it has a smaller threshold (by a factor of $2m_e/m_\pi \sim 10^{-2}$), it also has a smaller cross section. But, it becomes important at sub-GZK energies. Attenuation length for this reaction is 10^3 Mpc – a noticeable and important effect.

UHE photons loose energy in $\gamma + \gamma \to e^+e^-$. The threshold for the reaction with CMBR photons is smaller by a factor of $2m_e^2/m_\pi m_p \sim 10^{-5}$ compared to the GZK cutoff energy. The cross-section decreases fast with energy, $\sigma = \sigma_{\rm T} m_e/s^2$, where $\sqrt{s}$ is the CM energy and $\sigma_{\rm T} \approx 10^{-22}{\rm cm}^2$ is the Thomson cross-section. Therefore, attenuation length has a minimum at the pair production threshold. For CMBR photons, this occurs at $E \approx 2 \cdot 10^{14}$ eV and $L_A \approx 10$ kpc. The attenuation length increases with energy, reaching GZK distance roughly at $E \approx 10^{20}$ eV. Photons with even larger energies are able to penetrate even larger distances – and this is important for many models – but in this energy range, the main contribution comes from poorly known radio-background, which brings some uncertainty in the attenuation length of the highest energy photons.

Heavy nuclei loose energy in photo-dissociation. Here, the main contribution comes from the infra-red background which is also poorly known. But again, at $E \approx 10^{20}$ eV the attenuation length is comparable to the GZK distance [122].

The cut-off. It is easy to understand why a sharp cut-off in the spectrum of protons should appear. This happens because the attenuation length decreases rapidly with increasing energy. Assume a power law injection spectrum for UHECR, $J_{in}(E) \propto E^{-\alpha}$, and let $n(r)$ be the density of sources. Fluxes from individual sources decrease as r^{-2}, which is compensated by volume integration, $r^2 dr$. Therefore, the total flux registered at energy E should grow in proportion to the upper limit of volume integration

$$J(E) \propto \int_0^{R(E)} n(r) dr \ \propto \ R(E) \ , \tag{132}$$

if the distribution of sources, $n(r)$, does not depend on r. Here, $R(E)$ corresponds to the attenuation length, i.e. the distance from which cosmic rays with energy E can reach us. The attenuation length of protons with $E < 5 \times 10^{19}$ eV equals 10^3 Mpc, while the attenuation length at $E > 5 \cdot 10^{20}$ eV is only 10 Mpc. We conclude that

[**A2**] *The drop in flux by 2 orders of magnitude at GZK energy is expected if the distribution of sources is homogeneous .*

A word of caution is needed here. Transition in $R(E)$ from sub-GZK to super-GZK regime is not instantaneous. Therefore, a particular value of the drop depends upon the shape of the injection spectrum, i.e. on the value of α, see e.g. Refs. [123, 124, 125].

8.2 Generation of UHECR

The origin of cosmic rays and/or their acceleration mechanisms have been a subject of debate for several decades. Particles can be accelerated either by astrophysical shock waves, or by electric fields. In either case, one can estimate the maximum energy; with optimistic assumptions, the final estimate is the same for both mechanisms. In practice, the maximum of energy is expected to be much lower.

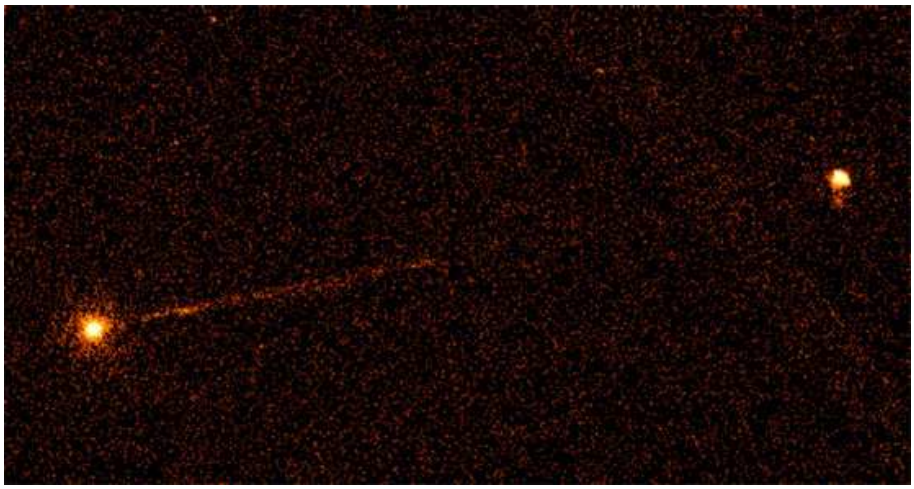

Fig. 23: *Chandra* telescope X-ray image of the nucleus, jet, and hot spot of Pictor A. From Ref. [127].

1. *Shock acceleration.* Particles are accelerated stochastically while bouncing between shocks. Acceleration can continue only if particles remain confined within an accelerating region, in other words until gyro-radius, Eq. (125), is smaller than the size of the region. This gives

$$E_{\max} = ZeBL \; . \tag{133}$$

2. *Acceleration by an electric field.* The latter can be created by a rapidly rotating magnetized neutron star or black hole. If motion is relativistic, the generated electric field is of the same order as the magnetic field, and the difference in electric potentials is $\sim (B \times L)$. This, again, reproduces Eq. (133) for the maximum energy.

Known astrophysical sources with $(B \times L)$ big enough to give $E_{\max} \sim 10^{20}$ eV are neutron stars, active galactic nuclei (AGN) and colliding galaxies.

The central engine of an AGN is believed to be a super-massive black hole powered by matter accretion. AGNs have two jets (one of the jets may be invisible because of the Doppler effect) of relativistic particles streaming in opposite directions. Interaction with the intergalactic medium terminates this motion and at the ends of jets the radio-lobes and hot-spots are formed, see Fig. 23. The acceleration of UHECR primaries may occur either near the black hole horizon (direct acceleration), or in hot spots of jets and radio-lobes (shock acceleration). The host of different AGNs is now classified in one unified scheme, for a review see [126]. Depending upon the angle between the jet axis and the line of sight we observe different types of AGN. A typical radio galaxy, showing two strong opposite jets, is observed at angles approximately perpendicular to the jet axis. An AGN is classified as a quasar if the angle is smaller than 30°. If we look along the jet axis (angle $< 10^\circ$), i.e. directly into the barrel of the gun, we observe a blazar.

It should be noted that not all radio-galaxies are the same. There are Fanaroff-Riley (FR) type I and type II galaxies (radio-loud AGNs), and Seyfert galaxies (radio-quiet AGNs). Both types of FR galaxies may be the sites of UHECR acceleration, but the hot spots in FR type II galaxies are considered to be most promising [128]. It is believed that when observed along the jet axis, FR type II galaxies make a parent population of Highly Polarized Quasars (HPQ – subclass of blazars), while FR type I galaxies make a parent population of BL Lacertae objects (BL Lacs – another subclass of blazars).

As an example, the X-ray image of the powerful FR-II radio galaxy Pictor A taken by *Chandra* observatory is shown in Fig. 23. Radio observations of jets have a long history. Recently, *Chandra* started to obtain high resolution X-ray maps of AGNs which, surprisingly, revealed very long collimated

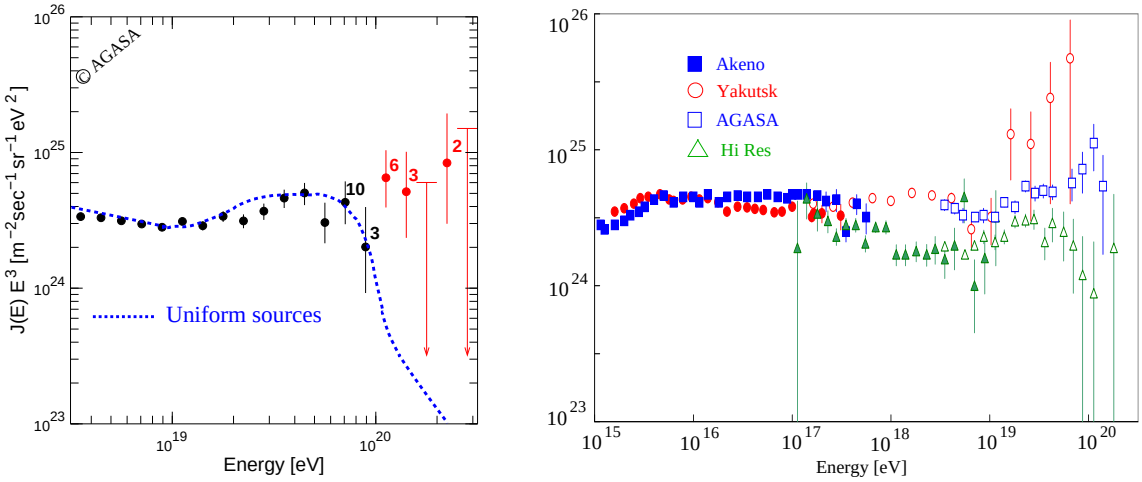

Fig. 24: **Left panel:** The energy spectrum of cosmic rays with a zenith angle up to 45° as measured by AGASA [108]. Numbers near data points reflect the number of events in the respective energy bins. **Right panel:** A compilation of data from different experiments: Akeno (filled squares), AGASA (open squares), HiRes-I and HiRes-II (open and filled triangles), two Yakutsk sub-arrays of Cherenkov detectors (open and filled circles). From Ref. [133].

X-ray jets. E.g. the distance from nucleus to the hot spot in Pictor A is at least 240 kpc. It is hard to explain such long jets as pure leptonic, and it is possible that the population of relativistic electrons responsible for the X-ray emission is a result of photo-pion production by UHE protons [127].

Now, for any acceleration mechanism and independent of the actual acceleration site (i.e. be it either the AGN's black hole or any of the hot spots) the momentum of highest energy particles is expected to point in the direction of the jet [129]. In other words, if AGNs are sources of UHECR, arrival directions of high energy cosmic rays may point back to a (subclass) of a blazar family. Such correlations were indeed observed [129, 130, 131, 132] with BL Lacertae objects.

8.3 UHECR spectrum.

The largest statistic of UHECR events has been accumulated for over 12 years of operation by the AGASA air shower array of surface particle detectors. The spectrum measured by the AGASA is shown in Fig. 24, left panel. The dotted curve represents the theoretical expectation for a homogeneous distribution of sources and proton primaries. This theoretical curve exhibits the GZK cut-off at $E \approx 10^{20}$ eV. Remarkably, AGASA had detected 11 events with higher energy and the data show no hint for cut-off.

It is hard to argue against the reality of these findings. AGASA exposure is under control, and the only issue is the energy determination. AGASA events have an accuracy of $\pm 25\%$ in event-reconstruction resolution and 18% in systematic errors around 10^{20} eV [108]. Added in quadrature this gives RMS error of energy determination to be $\pm 30\%$. More importantly, the probability of an upward fluctuation to 1.5 times the true energy is 2.8%. There are too many super-GZK events, and with this resolution a spectrum with GZK cutoff cannot be transformed into an excess of post-GZK events assuming spillover [112].

Recently, the HiRes group has reported results obtained with a telescope which measures atmospheric fluorescence light. The energy spectrum is shown in Fig. 24 by triangles, the right panel. The spectrum is consistent with the GZK cut-off, and there are 2 events detected with $E > 10^{20}$ eV. Systematic error in energy measurement was estimated to be 21%, systematic error in the aperture is not yet

clear. HiRes employs a relatively new technique, with the following issues usually cited for improvement: atmospheric attenuation corrections should be based on nightly measurements and not averages, better energy calibration and aperture calculation are called for, see e.g. [112].

The Yakutsk group uses a hybrid detection method, combining a ground array of particle detectors with telescopes which are measuring Cherenkov light produced by a shower in the atmosphere. A recently reported [133] spectrum, derived from air Cherenkov light measurements, is shown in the right panel of Fig. 24 by circles. At the low energy end it agrees well with the Akeno spectrum, and at the high energy end it is consistent, within errors, with the AGASA spectrum. Yakutsk and AGASA disagree significantly with HiRes at $E \sim 10^{18}$ eV were statistical errors are negligible, which points out to some systematics. AGASA and HiRes can be reconciled at $E < 10^{20}$ by e.g. -15% and $+15\%$ respective shift of energy [134]. The discrepancy between two experiments at $E > 10^{20}$ after the shift is only 2σ. However, even after these shifts there are still 9 events with $E > 10^{20}$ in the combined data set.

8.4 The Puzzle

These measurements are regarded as a threefold puzzle, because contrary to assertions [A1], [A2]

[**P1**] No candidate sources are found within the GZK distance in the directions of $E > 10^{20}$ eV events;

[**P2**] The AGASA spectrum does not exhibit the GZK cutoff.

And finally we have the third puzzling question:

[**P3**] Which physical processes are capable of producing events with these enormous energies ?

Conjectures. With the assumption that all three pieces of the puzzle, [P1] – [P3], are correct, the situation becomes desperate. There were no solutions suggested which would not invoke new physics beyond the standard model, or very speculative astrophysics. In addition, all models require fine tuning, and many do not really solve all three problems. It is not possible to consider here all the suggested solutions. Ignoring for now the problem [P2], the situation with [P1] and [P3] does not become easier, but we can now restrict ourselves to the discussion of astrophysical solutions only.

Ignoring in addition [P3], the simplest suggestion is to assume very large extra-galactic magnetic fields, which would randomize UHECR trajectories. However, the results of Ref. [117] do not support such a conjecture. As we have mentioned already, a consensus regarding EGMF fields has not yet been reached and in Ref. [121], much stronger extragalactic magnetic fields were advocated. Nevertheless, even in this case, the conclusion was that the condition of global isotropy of UHECR arrival directions requires the "local" value of magnetic field to be rather weak, $B \lesssim 0.1\ \mu$G, which, in turn, leads to a large number of UHECR sources in the GZK volume, $n \gtrsim 100$; for similar limits on the number of sources see also Refs. [135, 136, 137, 138]. These weak EGMFs of Refs. [117, 121] rule out the possibility of a single powerful radio-galaxy, which happened to be nearby [139], or a gamma-ray burst scenario [140], as a potential sources of UHECR.

Another suggested astrophysical scenario was a "dead quasars" model [141]. This model assumes that quasars, powerful in the past, retain the possibility to accelerate to the highest energies even after the accretion of matter is exhausted and a quasar cease to be visible electromagnetically. However, the process of acceleration to the highest energies in compact sources is inevitably accompanied by a strong TeV emission [142]. Recent results obtained by several TeV telescopes, in particular, non-observation of strong TeV sources, rule out the "dead quasar" model [143]. In addition, in Ref. [144] it was found that known quasar remnants are typically distributed too anisotropically to explain the isotropic ultra high energy cosmic ray flux except in the unrealistic case where extragalactic magnetic fields of $0.1\ \mu$G extend over many Mpc.

A possibility that ultra-high-energy events are due to iron nuclei accelerated from young, strongly magnetized neutron stars in relativistic MHD winds has also been suggested [145]. However, with

realistic parameters of Galactic magnetic field, even iron nuclei do not propagate diffusively within Galaxy, which disfavors this model [146].

Any observational clue? Many quite different models were suggested for the resolution of the GZK puzzle. The majority of suggested models, which we have no space to consider here, employ a new physics of one sort or another. (The reader may consult UHECR reviews cited at the beginning of this section, but I believe that a review which would cover all the suggested possibilities does not exist.) Instead, let us consider the question of whether or not there is already a clue in the data as to which model may be correct. Hints, and, in principle, critical signatures are given by:

- *Spectral shape.* We do not yet have enough data at the highest energies to constrain models. Spectra below 10^{20} eV point to the AGN model of UHECR origin, with protons being primaries [147, 148].
- *Chemical composition.* Again, not enough data at the highest energies. An analysis of Haverah Park data at lower energies shows that above 10^{19} eV, less than 30% of the primary cosmic rays can be photons or iron nuclei at the 95% confidence level [149]. In other words, at least 70% should be protons.
- *Large-scale anisotropy.* Gives strong signatures. Not observed, which is a hint by itself. Some implications we had considered already, and may add that the non-observation of anisotropy towards the Galactic center has a potential of ruling out the model of UHECR origin based on decays of super-heavy dark matter [150, 151, 152, 153].
- *Small-scale clustering.* This is an observed [154], reliable feature. (Errors in angle determination are definitely small.) It is already statistically significant. Therefore, below I shall concentrate on this signature.

Small-scale clustering. It was observed by different installations that arrival directions of UHECR are too close to each other and this happens too often [155, 154, 156, 157]. In particular, the AGASA collaboration has observed 6 doublets and 1 triplet of cosmic rays with $E > 4 \times 10^{19}$ within 2.5°. The chance probability of observing just a triplet under an isotropic distribution is only 0.9% [154]. Statistical significance of these clusters in the AGASA data set was considered by several authors. In Ref. [157], an analysis based on the calculation of an angular autocorrelation function was employed, and the probability $P = 3 \times 10^{-4}$ of chance clustering was obtained. This includes the penalty for the choice of the energy cut, while the angular bin was chosen to be fixed at 2.5°, which is a value previously accepted by AGASA, being consistent with the angular resolution. In Ref. [158], this analysis was repeated and confirmed. In addition, two more conservative estimates were done. In the first, the penalty factor for the adjustment of the angular bin size was added. This returns $P = 3 \times 10^{-3}$. This is a valid procedure, but it misses prior information about the angular resolution of the installation. In the second estimate, the bin size was kept fixed, but the whole data set was divided in halves. The "original data set" [155] was used to justify the bin size of 2.5°, while clusters in it were removed for the subsequent evaluation of statistical significance. This procedure returned $P = 8 \times 10^{-2}$. Again, this is a valid approach too, and can be safely used with future large data sets. However, I'd like to stress that it is *not* an evaluation of the statistical significance of 6 doublets and 1 triplet. It is no wonder that a smaller data set has reduced statistical significance. Finally, in Ref. [159] it was found that the AGASA data set manifests a $P \sim 10^{-3}$ chance probability of clustering above background using independent statistics of $\langle \cos\theta \rangle_{[0^\circ, 10^\circ]}$. I find this value, $P \sim 10^{-3}$, to be fair estimate of the current significance of clustering in the AGASA data.

Note the following: if clusters are real and due to sources, the number of events in "physical" clusters should be Poisson distributed. Therefore, with the current low statistics, it is expected that roughly half of installations should observe significant clustering, while another half should not see it

[157]. There is no clustering in the current HiRes data [160, 159]. However, with the current statistics there is no contradiction yet [161, 159].

The study of small-scale clustering is very important. If clusters are real and not a statistical fluctuation, then UHECR should point back to sources and UHECR astronomy is possible. Real sources should be behind the clusters and the correlation studies make sense. Pursuing this strategy, one should be restricted to astrophysical sources with physical conditions potentially suitable for particle acceleration to the highest energies. Active galactic nuclei (AGN) constitute a particularly attractive class of potential sources. As we have already discussed, if AGNs are sources, those which have jets directed along the line of sight, or blazars, should correlate with observed UHECR events. It is intriguing that statistically significant correlations of UHECR with BL Lacertae objects were found [129].

9. Conclusions

Cosmology and astrophysics give us firm evidence that the standard model of particle physics is limited. The standard model fails to explain baryogenesis, does not contain non-baryonic dark matter and has no room for massive neutrino. We now know that dark energy also exists, but we do not know why it exists. There seems to be too many coincidences between numerical values of cosmological parameters which describe the matter and energy budget. Contributions of baryonic matter, non-baryonic matter and dark energy are almost equal at the present epoch, while they have seemingly unrelated origin and could differ by many orders of magnitude. Cosmology just became a precision science and is already full of surprises; we can expect even more exciting discoveries in the near future.

ACKNOWLEDGEMENTS

I would like to thank the conference organizers for friendly and warm atmosphere.

References

[1] G. Gabadadze, *Beyond the Standard Model.* (2003 European School of High-Energy Physics, Tsakhkadzor, Armenia, 24 August-6 September, 2003).

[2] S. Petcov, *Massive Neutrinos and Neutrino Oscillations.* (2003 European School of High-Energy Physics, Tsakhkadzor, Armenia, 24 August-6 September, 2003).

[3] A. Chilingaryan, *Galactic and Solar Cosmic Rays.* (2003 European School of High-Energy Physics, Tsakhkadzor, Armenia, 24 August-6 September, 2003).

[4] V. Rubakov, *Cosmology and Astrophysics.* (Proc. 2001 European School of High-Energy Physics, Beatenberg, Switzerland, 26 Aug - 8 Sept, 2001).

[5] M. Shaposhnikov, *Cosmology and Astrophysics.* (Proc. 2000 European School of High-Energy Physics, Caramulo, Portugal, 20 Aug - 2 Sep, 2000).

[6] J. Garcia-Bellido, *Astrophysics and Cosmology.* (Proc. 1999 European School of High-Energy Physics, Casta-Papernicka, Slovak Republic, 22 Aug - 4 Sep, 1999), hep-ph/0004188.

[7] K. A. Olive, G. Steigman, and T. P. Walker, Phys. Rept. **333**, 389 (2000), astro-ph/9905320.

[8] V. A. Rubakov and M. E. Shaposhnikov, Usp. Fiz. Nauk **166**, 493 (1996), hep-ph/9603208.

[9] C. L. Bennett *et al.*, Astrophys. J. Suppl. **148**, 1 (2003), astro-ph/0302207.

[10] SDSS, M. Tegmark *et al.*, (2003), astro-ph/0310723.

[11] A. G. Riess *et al.*, (2004), astro-ph/0402512.

[12] D. J. Schwarz, Annalen Phys. **12**, 220 (2003), astro-ph/0303574.

[13] B. M. S. Hansen *et al.*, Astrophys. J. **574**, L155 (2002).

[14] W. L. Freedman *et al.*, Astrophys. J. **553**, 47 (2001), astro-ph/0012376.

[15] A. A. Penzias and R. W. Wilson, Astrophys. J. **142**, 419 (1965).

[16] R. H. Dicke, P. J. E. Peebles, P. G. Roll, and D. T. Wilkinson, Astrophys. J. **142**, 414 (1965).

[17] T. Shmaonov, Pribori Tekhnika Eksperimenta **1**, 83 (1957).

[18] A. McKellar, Proc. Ast. Soc. Pac. **52**, 187 (1940).

[19] A. G. Doroshkevich and I. D. Novikov, Sov. Phys. Dokl. **9**, 111 (1964).

[20] D. J. Fixsen *et al.*, Astrophys. J. **473**, 576 (1996), astro-ph/9605054.

[21] M. Kamionkowski and L. Knox, Phys. Rev. **D67**, 063001 (2003), astro-ph/0210165.

[22] C. L. Bennett *et al.*, Astrophys. J. **464**, L1 (1996), astro-ph/9601067.

[23] G. F. Smoot *et al.*, Astrophys. J. **396**, L1 (1992).

[24] R. K. Sachs and A. M. Wolfe, Astrophys. J. **147**, 73 (1967).

[25] J. Silk, Astrophys. J. **151**, 459 (1968).

[26] P. J. E. Peebles and J. T. Yu, Astrophys. J. **162**, 815 (1970).

[27] R. A. Syunyaev and Y. B. Zel'Dovich, Astrophysics and Space Science **7**, 3 (1970).

[28] A. G. Doroshkevich, Y. B. Zel'Dovich, and R. A. Syunyaev, Soviet Astronomy **22**, 523 (1978).

[29] W. Hu and S. Dodelson, Ann. Rev. Astron. Astrophys. **40**, 171 (2002), astro-ph/0110414.

[30] W. Hu and M. J. White, Phys. Rev. Lett. **77**, 1687 (1996), astro-ph/9602020.

[31] F. R. Bouchet, P. Peter, A. Riazuelo, and M. Sakellariadou, Phys. Rev. **D65**, 021301 (2002), astro-ph/0005022.

[32] D. Huterer and M. S. Turner, Phys. Rev. **D64**, 123527 (2001), astro-ph/0012510.

[33] Supernova Search Team, A. G. Riess *et al.*, Astron. J. **116**, 1009 (1998), astro-ph/9805201.

[34] D. N. Spergel *et al.*, Astrophys. J. Suppl. **148**, 175 (2003), astro-ph/0302209.

[35] G. Soucail, J. P. Kneib, and G. Golse, (2004), astro-ph/0402658.

[36] E. Corbelli and P. Salucci, (1999), astro-ph/9909252.

[37] K. G. Begeman, A. H. Broeils, and R. H. Sanders, MNRAS **249**, 523 (1991).

[38] J. F. Navarro, C. S. Frenk, and S. D. M. White, Astrophys. J. **490**, 493 (1997).

[39] S. Ghigna *et al.*, Astrophys. J. **544**, 616 (2000), astro-ph/9910166.

[40] P. Sikivie, I. I. Tkachev, and Y. Wang, Phys. Rev. **D56**, 1863 (1997), astro-ph/9609022.

[41] G. Steigman and I. Tkachev, (1998), astro-ph/9803008.

[42] W. H. Kinney and P. Sikivie, Phys. Rev. **D61**, 087305 (2000), astro-ph/9906049.

[43] C. Charmousis, V. Onemli, Z. Qiu, and P. Sikivie, Phys. Rev. **D67**, 103502 (2003), astro-ph/0301399.

[44] D. P. Bennett *et al.*, Astrophys. J. **579**, 639 (2002), astro-ph/0109467.

[45] EROS, C. Afonso *et al.*, Astron. Astrophys. **400**, 951 (2003), astro-ph/0212176.

[46] P. Popowski *et al.*, (2003), astro-ph/0304464.

[47] J. Yoo, J. Chaname, and A. Gould, Astrophys. J. **601**, 311 (2004), astro-ph/0307437.

[48] F. Zwicky, Helv. Phys. Acta **6**, 110 (1933).

[49] A. D. Lewis, D. A. Buote, and J. T. Stocke, Astrophys. J. **586**, 135 (2003), astro-ph/0209205.

[50] Carlberg *et al.*, Astrophys. J. **462**, 32 (1996), astro-ph/9509034.

[51] M. Loewenstein and R. Mushotzky, (2002), astro-ph/0208090.

[52] J. P. Kneib, R. S. Ellis, I. Smail, W. J. Couch, and R. M. Sharples, Astrophys. J. **471**, 643 (1996), astro-ph/9511015.

[53] M. Bartelmann and P. Schneider, Physics Reports **340**, 291 (2001), astro-ph/9912508.

[54] G. Squires *et al.*, Astrophys. J. **461**, 572 (1996), astro-ph/9507008.

[55] S. Weinberg, Phys. Rev. Lett. **40**, 223 (1978).

[56] F. Wilczek, Phys. Rev. Lett. **40**, 279 (1978).

[57] R. D. Peccei and H. R. Quinn, Phys. Rev. Lett. **38**, 1440 (1977).

[58] G. G. Raffelt, Phys. Rept. **198**, 1 (1990).

[59] R. Bradley *et al.*, Rev. Mod. Phys. **75**, 777 (2003).

[60] A. D. Dolgov, Phys. Rept. **370**, 333 (2002), hep-ph/0202122.

[61] G. G. Raffelt, Ann. Rev. Nucl. Part. Sci. **49**, 163 (1999), hep-ph/9903472.

[62] S. I. Blinnikov and M. Y. Khlopov, Sov. J. Nucl. Phys. **36**, 472 (1982).

[63] Z. Berezhiani, D. Comelli, and F. L. Villante, Phys. Lett. **B503**, 362 (2001), hep-ph/0008105.

[64] R. Foot and R. R. Volkas, Phys. Rev. **D68**, 021304 (2003), hep-ph/0304261.

[65] K. A. Olive, (2003), astro-ph/0301505.

[66] J. R. Ellis, (2003), astro-ph/0305038.

[67] P. Gondolo, (2004), astro-ph/0403064.

[68] V. Berezinsky, M. Kachelriess, and A. Vilenkin, Phys. Rev. Lett. **79**, 4302 (1997), astro-ph/9708217.

[69] V. A. Kuzmin and V. A. Rubakov, Phys. Atom. Nucl. **61**, 1028 (1998), astro-ph/9709187.

[70] D. J. H. Chung, E. W. Kolb, and A. Riotto, Phys. Rev. **D59**, 023501 (1999), hep-ph/9802238.

[71] V. Kuzmin and I. Tkachev, JETP Lett. **68**, 271 (1998), hep-ph/9802304.

[72] G. Jungman, M. Kamionkowski, and K. Griest, Phys. Rept. **267**, 195 (1996), hep-ph/9506380.

[73] DAMA, R. Bernabei *et al.*, Phys. Lett. **B480**, 23 (2000).

[74] CDMS, D. S. Akerib *et al.*, (2004), astro-ph/0405033.

[75] S. S. Gershtein and Y. B. Zeldovich, JETP Lett. **4**, 120 (1966).

[76] G. Bhattacharyya, H. Paes, L.-g. Song, and T. J. Weiler, Phys. Lett. **B564**, 175 (2003), hep-ph/0302191.

[77] S. Tremaine and J. E. Gunn, Phys. Rev. Lett. **42**, 407 (1979).

[78] K. Griest and M. Kamionkowski, Phys. Rev. Lett. **64**, 615 (1990).

[79] C. J. Hogan and M. J. Rees, Phys. Lett. **B205**, 228 (1988).

[80] E. W. Kolb and I. I. Tkachev, Phys. Rev. Lett. **71**, 3051 (1993), hep-ph/9303313.

[81] E. W. Kolb and I. I. Tkachev, Astrophys. J. **460**, L25 (1996), astro-ph/9510043.

[82] L. F. Abbott and P. Sikivie, Phys. Lett. **B120**, 133 (1983).

[83] M. Dine and W. Fischler, Phys. Lett. **B120**, 137 (1983).

[84] V. Kuzmin and I. Tkachev, Phys. Rev. **D59**, 123006 (1999), hep-ph/9809547.

[85] A. A. Starobinsky, Phys. Lett. **B91**, 99 (1980).

[86] A. H. Guth, Phys. Rev. **D23**, 347 (1981).

[87] A. D. Linde, Phys. Lett. **B108**, 389 (1982).

[88] A. Albrecht and P. J. Steinhardt, Phys. Rev. Lett. **48**, 1220 (1982).

[89] A. D. Linde, Phys. Lett. **B129**, 177 (1983).

[90] A. H. Guth and E. J. Weinberg, Phys. Rev. **D23**, 876 (1981).

[91] A. R. Liddle and D. H. Lyth, Phys. Rept. **231**, 1 (1993), astro-ph/9303019.

[92] L. P. Grishchuk, Sov. Phys. JETP **40**, 409 (1975).

[93] V. N. Lukash, Sov. Phys. JETP **52**, 807 (1980).

[94] M. Sasaki, Prog. Theor. Phys. **76**, 1036 (1986).

[95] V. F. Mukhanov, Sov. Phys. JETP **67**, 1297 (1988).

[96] V. F. Mukhanov, H. A. Feldman, and R. H. Brandenberger, Phys. Rept. **215**, 203 (1992).

[97] V. A. Rubakov, M. V. Sazhin, and A. V. Veryaskin, Phys. Lett. **B115**, 189 (1982).

[98] E. R. Harrison, Phys. Rev. **D1**, 2726 (1970).

[99] Y. B. Zeldovich, Mon. Not. Roy. Astron. Soc. **160**, 1 (1972).

[100] J. E. Lidsey *et al.*, Rev. Mod. Phys. **69**, 373 (1997), astro-ph/9508078.

[101] K. Greisen, Phys. Rev. Lett. **16**, 748 (1966).

[102] G. T. Zatsepin and V. A. Kuzmin, JETP Lett. **4**, 78 (1966).

[103] J. Linsley, Phys. Rev. Lett. **10**, 146 (1963).

[104] M. M. Winn, J. Ulrichs, L. S. Peak, C. B. A. Mccusker, and L. Horton, J. Phys. **G12**, 653 (1986).

[105] M. A. Lawrence, R. J. O. Reid, and A. A. Watson, J. Phys. **G17**, 733 (1991).

[106] A. V. Glushkov *et al.*, Bull. Russ. Acad. Sci. Phys. **55**, NO.495 (1991).

[107] D. J. Bird *et al.*, Astrophys. J. **441**, 144 (1995).

[108] M. Takeda *et al.*, Astropart. Phys. **19**, 447 (2003), astro-ph/0209422.

[109] High Resolution Fly's Eye, T. Abu-Zayyad *et al.*, (2002), astro-ph/0208301.

[110] M. Nagano and A. A. Watson, Rev. Mod. Phys. **72**, 689 (2000).

[111] L. Anchordoqui, T. Paul, S. Reucroft, and J. Swain, Int. J. Mod. Phys. **A18**, 2229 (2003), hep-ph/0206072.

[112] J. W. Cronin, (2004), astro-ph/0402487.

[113] D. F. Torres and L. A. Anchordoqui, (2004), astro-ph/0402371.

[114] N. N. Kalmykov and S. S. Ostapchenko, Phys. Atom. Nucl. **56**, 346 (1993).

[115] K.-H. Kampert, Heavy Ion Phys. **14**, 203 (2001), astro-ph/0101331.

[116] M. Ave, J. A. Hinton, R. A. Vazquez, A. A. Watson, and E. Zas, Phys. Rev. **D65**, 063007 (2002), astro-ph/0110613.

[117] K. Dolag, D. Grasso, V. Springel, and I. Tkachev, (2003), astro-ph/0310902.

[118] C. L. Carilli and G. B. Taylor, Ann. Rev. Astron. Astrophys. **40**, 319 (2002), astro-ph/0110655.

[119] P. P. Kronberg, Rept. Prog. Phys. **57**, 325 (1994).

[120] P. Blasi, S. Burles, and A. V. Olinto, Astrophys. J. **514**, L79 (1999), astro-ph/9812487.

[121] G. Sigl, F. Miniati, and T. A. Ensslin, (2004), astro-ph/0401084.

[122] F. W. Stecker and M. H. Salamon, Astrophys. J. **512**, 521 (1999), astro-ph/9808110.

[123] M. Blanton, P. Blasi, and A. V. Olinto, Astropart. Phys. **15**, 275 (2001), astro-ph/0009466.

[124] O. E. Kalashev, V. A. Kuzmin, D. V. Semikoz, and I. I. Tkachev, (2001), astro-ph/0107130.

[125] V. Berezinsky, A. Z. Gazizov, and S. I. Grigorieva, (2001), hep-ph/0107306.

[126] C. M. Urry and P. Padovani, Publ. Astron. Soc. Pac. **107**, 803 (1995), astro-ph/9506063.

[127] A. S. Wilson, A. J. Young, and P. L. Shopbell, Astrophys. J. **547**, 740 (2001), astro-ph/0008467.

[128] J. P. Rachen and P. L. Biermann, Astron. Astrophys. **272**, 161 (1993), astro-ph/9301010.

[129] P. G. Tinyakov and I. I. Tkachev, JETP Lett. **74**, 445 (2001), astro-ph/0102476.

[130] P. G. Tinyakov and I. I. Tkachev, Astropart. Phys. **18**, 165 (2002), astro-ph/0111305.

[131] D. S. Gorbunov, P. G. Tinyakov, I. I. Tkachev, and S. V. Troitsky, Astrophys. J. **577**, L93 (2002), astro-ph/0204360.

[132] P. Tinyakov and I. Tkachev, (2003), astro-ph/0305363.

[133] A. A. Ivanov, S. P. Knurenko, and I. Y. Sleptsov, Nucl. Phys. Proc. Suppl. **122**, 226 (2003), astro-ph/0305053.

[134] D. De Marco, P. Blasi, and A. V. Olinto, Astropart. Phys. **20**, 53 (2003), astro-ph/0301497.

[135] S. L. Dubovsky, P. G. Tinyakov, and I. I. Tkachev, Phys. Rev. Lett. **85**, 1154 (2000), astro-ph/0001317.

[136] Z. Fodor and S. D. Katz, Phys. Rev. **D63**, 023002 (2001), hep-ph/0007158.

[137] P. Blasi and D. De Marco, Astropart. Phys. **20**, 559 (2004), astro-ph/0307067.

[138] D. Harari, S. Mollerach, and E. Roulet, (2004), astro-ph/0404304.

[139] G. R. Farrar and T. Piran, (2000), astro-ph/0010370.

[140] E. Waxman, Phys. Rev. Lett. **75**, 386 (1995), astro-ph/9505082.

[141] E. Boldt and P. Ghosh, MNRAS **307**, 491 (1999), astro-ph/9902342.

[142] A. Levinson, Phys. Rev. Lett. **85**, 912 (2000).

[143] A. Neronov, P. Tinyakov, and I. Tkachev, (2004), astro-ph/0402132.

[144] C. Isola, G. Sigl, and G. Bertone, (2003), astro-ph/0312374.

[145] P. Blasi, R. I. Epstein, and A. V. Olinto, Astrophys. J. **533**, L123 (2000), astro-ph/9912240.

[146] S. O'Neill, A. V. Olinto, and P. Blasi, (2001), astro-ph/0108401.

[147] V. Berezinsky, A. Z. Gazizov, and S. I. Grigorieva, (2002), hep-ph/0204357.

[148] V. Berezinsky, A. Z. Gazizov, and S. I. Grigorieva, (2002), astro-ph/0210095.

[149] M. Ave, J. A. Hinton, R. A. Vazquez, A. A. Watson, and E. Zas, Phys. Rev. Lett. **85**, 2244 (2000), astro-ph/0007386.

[150] S. L. Dubovsky and P. G. Tinyakov, JETP Lett. **68**, 107 (1998), hep-ph/9802382.

[151] V. Berezinsky and A. A. Mikhailov, Phys. Lett. **B449**, 237 (1999), astro-ph/9810277.

[152] H. B. Kim and P. Tinyakov, (2003), astro-ph/0306413.

[153] M. Kachelriess and D. V. Semikoz, Phys. Lett. **B577**, 1 (2003), astro-ph/0306282.

[154] AGASA, M. Takeda *et al.*, Astrophys. J. **522**, 225 (1999), astro-ph/9902239.

[155] AGASA, N. Hayashida *et al.*, Phys. Rev. Lett. **77**, 1000 (1996).

[156] Y. Uchihori *et al.*, Astropart. Phys. **13**, 151 (2000), astro-ph/9908193.

[157] P. G. Tinyakov and I. I. Tkachev, JETP Lett. **74**, 1 (2001), astro-ph/0102101.

[158] C. B. Finley and S. Westerhoff, (2003), astro-ph/0309159.

[159] The High Resolution Fly's Eye (HIRES), R. U. Abbasi *et al.*, (2004), astro-ph/0404366.

[160] The High Resolution Fly's Eye (HIRES), R. U. Abbasi *et al.*, (2004), astro-ph/0404137.

[161] H. Yoshiguchi, S. Nagataki, and K. Sato, (2004), astro-ph/0404411.